U. of Iowa 71:19

N71-33392
NASA CR-121418

VLF Hiss and Related Plasma Observations in the Polar Magnetosphere

by

D. A. Gurnett and L. A. Frank

Department of Physics and Astronomy
THE UNIVERSITY OF IOWA
Iowa City, Iowa

UNCLASSIFIED

Security Classification

DOCUMENT CONTROL DATA - R&D

(Security classification of title, body of abstract and indexing annotation must be entered when the overall report is classified)

1 ORIGINATING ACTIVITY *(Corporate author)*

Department of Physics & Astronomy
University of Iowa

2a. REPORT SECURITY CLASSIFICATION

UNCLASSIFIED

2b GROUP

3. REPORT TITLE

"VLF Hiss and Related Plasma Observations in the Polar Magnetosphere"

4. DESCRIPTIVE NOTES *(Type of report and inclusive dates)*

Progress, May 1971

5 AUTHOR(S) *(Last name, first name, initial)*

Gurnett, Donald A. and Louis A. Frank

6. REPORT DATE	7a. TOTAL NO. OF PAGES	7b. NO. OF REFS
May 1971	58	21

8a. CONTRACT OR GRANT NO.	9a. ORIGINATOR'S REPORT NUMBER(S)
N00014-68-A-0196-0003	U. of Iowa 71-19
b. PROJECT NO.	
c.	9b. OTHER REPORT NO(S) *(Any other numbers that may be assigned this report)*
d.	

10. AVAILABILITY/LIMITATION NOTICES

Distribution of this document is unlimited.

11. SUPPLEMENTARY NOTES	12. SPONSORING MILITARY ACTIVITY
	Office of Naval Research

13. ABSTRACT

[See following page]

DD FORM 1 JAN 64 1473

UNCLASSIFIED

Security Classification

14. KEY WORDS	LINK A		LINK B		LINK C	
	ROLE	WT	ROLE	WT	ROLE	WT
Auroral Zone VLF Hiss						
Polar Cusp Plasma						
Upgoing Electron Fluxes						

INSTRUCTIONS

1. ORIGINATING ACTIVITY: Enter the name and address of the contractor, subcontractor, grantee, Department of Defense activity or other organization *(corporate author)* issuing the report.

2a. REPORT SECURITY CLASSIFICATION: Enter the overall security classification of the report. Indicate whether "Restricted Data" is included. Marking is to be in accordance with appropriate security regulations.

2b. GROUP: Automatic downgrading is specified in DoD Directive 5200.10 and Armed Forces Industrial Manual. Enter the group number. Also, when applicable, show that optional markings have been used for Group 3 and Group 4 as authorized.

3. REPORT TITLE: Enter the complete report title in all capital letters. Titles in all cases should be unclassified. If a meaningful title cannot be selected without classification, show title classification in all capitals in parenthesis immediately following the title.

4. DESCRIPTIVE NOTES: If appropriate, enter the type of report, e.g., interim, progress, summary, annual, or final. Give the inclusive dates when a specific reporting period is covered.

5. AUTHOR(S): Enter the name(s) of author(s) as shown on or in the report. Enter last name, first name, middle initial. If military, show rank and branch of service. The name of the principal author is an absolute minimum requirement.

6. REPORT DATE: Enter the date of the report as day, month, year; or month, year. If more than one date appears on the report, use date of publication.

7a. TOTAL NUMBER OF PAGES: The total page count should follow normal pagination procedures, i.e., enter the number of pages containing information.

7b. NUMBER OF REFERENCES: Enter the total number of references cited in the report.

8a. CONTRACT OR GRANT NUMBER: If appropriate, enter the applicable number of the contract or grant under which the report was written.

8b, 8c, & 8d. PROJECT NUMBER: Enter the appropriate military department identification, such as project number, subproject number, system numbers, task number, etc.

9a. ORIGINATOR'S REPORT NUMBER(S): Enter the official report number by which the document will be identified and controlled by the originating activity. This number must be unique to this report.

9b. OTHER REPORT NUMBER(S): If the report has been assigned any other report numbers *(either by the originator or by the sponsor)*, also enter this number(s).

10. AVAILABILITY/LIMITATION NOTICES: Enter any limitations on further dissemination of the report, other than those imposed by security classification, using standard statements such as:

(1) "Qualified requesters may obtain copies of this report from DDC."

(2) "Foreign announcement and dissemination of this report by DDC is not authorized."

(3) "U. S. Government agencies may obtain copies of this report directly from DDC. Other qualified DDC users shall request through _____."

(4) "U. S. military agencies may obtain copies of this report directly from DDC. Other qualified users shall request through _____."

(5) "All distribution of this report is controlled. Qualified DDC users shall request through _____."

If the report has been furnished to the Office of Technical Services, Department of Commerce, for sale to the public, indicate this fact and enter the price, if known.

11. SUPPLEMENTARY NOTES: Use for additional explanatory notes.

12. SPONSORING MILITARY ACTIVITY: Enter the name of the departmental project office or laboratory sponsoring *(paying for)* the research and development. Include address.

13. ABSTRACT: Enter an abstract giving a brief and factual summary of the document indicative of the report, even though it may also appear elsewhere in the body of the technical report. If additional space is required, a continuation sheet shall be attached.

It is highly desirable that the abstract of classified reports be unclassified. Each paragraph of the abstract shall end with an indication of the military security classification of the information in the paragraph, represented as *(TS)*, *(S)*, *(C)*, or *(U)*.

There is no limitation on the length of the abstract. However, the suggested length is from 150 to 225 words.

14. KEY WORDS: Key words are technically meaningful terms or short phrases that characterize a report and may be used as index entries for cataloging the report. Key words must be selected so that no security classification is required. Identifiers, such as equipment model designation, trade name, military project code name, geographic location, may be used as key words but will be followed by an indication of technical context. The assignment of links, roles, and weights is optional.

U. of Iowa 71-19

VLF Hiss and Related Plasma Observations in the Polar Magnetosphere

by

D. A. Gurnett and L. A. Frank

Department of Physics and Astronomy
The University of Iowa
Iowa City, Iowa 52240

May 1971

Research supported in part by the National Aeronautics and Space Administration under contracts NAS5-10625, NAS1-8141, NAS1-8144(f), NAS1-8150(f), and NGL-16-001-043(97), and by the Office of Naval Research under contract N00014-68-A-0196-0003.

ABSTRACT

This paper presents a study of auroral zone VLF hiss and low-energy charged particle observations with the Injun 5 satellite. The results of this study provide the first direct verification of the association between auroral zone VLF hiss and intense fluxes, 10^4 to 10^7 electrons $(cm^2\text{-sec-sr-eV})^{-1}$, of low energy electrons with energies on the order of 100 eV to several keV. On the dayside of the magnetosphere, these low-energy electrons are identified with the dayside polar cusp region observed at higher latitudes with the IMP-5 satellite. At other local times, through the dawn and dusk regions and into the nightside of the magnetosphere, the VLF hiss and low-energy electron precipitation regions are believed to correspond to the extension of the dayside polar cusp into the distant plasma sheet and downstream magnetosheath on the nightside of the magnetosphere. Intense fluxes of upgoing electrons are often observed in a narrow latitudinal band near the low-energy electron precipitation bands. These upgoing electrons are believed to be associated with another type of VLF emission called a saucer, which is frequently observed with Injun 5.

On the basis of present models, the observed VLF hiss intensities cannot be accounted for by incoherent Cerenkov radiation from the observed electron fluxes, indicating that a coherent plasma instability mechanism is involved in some, if not all, of the VLF hiss generation. A model for the generation regions of VLF hiss and saucer emissions is discussed.

I. INTRODUCTION

Intense broad-band VLF and LF radio noise emissions, called "VLF hiss" or "auroral hiss" are commonly observed at high latitudes with both ground and satellite instrumentation [see for example, Helliwell, 1965; Gurnett, 1966; McEwen and Barrington, 1967; and Laaspere et al., 1971]. The frequency spectrum of these VLF hiss emissions is often very broad, extending in some cases from less than 1 kHz to greater than 500 kHz. The maximum power spectral densities of auroral hiss are on the order of 10^{-14} to 10^{-12} watt $(m^2\text{-}Hz)^{-1}$ [Gurnett, 1966; Jørgensen, 1968]. Since VLF hiss cannot propagate in the whistler mode at frequencies greater than the local electron gyrofrequency, it follows that the auroral zone VLF hiss emissions must be generated at relatively low altitudes in the polar magnetosphere, less than 5 earth radii for 10 kHz and less than 2 earth radii for 100 kHz.

Ellis [1959] first proposed that auroral zone VLF hiss emissions may be produced by incoherent Cerenkov radiation from the same charged particles which produce auroras. Initial estimates by Ellis based on the limited information about auroral charged particle energies and fluxes available at that time indicated that the incoherent

Cerenkov radiation process was several orders of magnitude too low to explain the observed power fluxes. However, later, in a more complete analysis based on more recent data, this conclusion was revised by Jørgensen [1968] who concluded that VLF hiss could be generated by incoherent Cerenkov radiation from large, but plausible, fluxes of electrons with energies of the order of 1 keV.

Because suitable simultaneous measurements of low-energy charged particle fluxes and VLF radio noise have not been available, it has not been previously possible to identify the charged particles responsible for the generation of auroral zone VLF hiss. Gurnett [1966], using data from the Injun 3 satellite, made the first quantitative investigation of charged particle fluxes and their association with auroral zone VLF hiss. Gurnett found that the VLF hiss emissions were essentially anti-correlated with the intensities of electrons with energies $E \geq 40$ keV, and that the VLF hiss usually occurred on the high latitude side of the trapping boundary for electrons $E \geq 40$ keV. In a few cases, excellent correlations were found between the occurrence of VLF hiss and very intense fluxes of electrons with energies $E \gtrsim 10$ keV. Generally, however, the charged particles responsible for the auroral zone VLF hiss emissions could not be detected because of the poor sensitivity and limited energy range of the Injun 3 instrumentation.

Recently Laaspere et al., [1971] and Hartz [1971] have suggested that VLF hiss on the dayside of the magnetosphere is associated with an influx of low-energy, 0.1 to 1.0 keV, electrons in a region identified as the "soft" electron precipitation zone by Johnson and Sharp [1969] and by Eather [1969]. In this paper we present the first study of auroral zone VLF hiss with charged particle and VLF instrumentation of suitable sensitivities and dynamic ranges to clearly identify the charged particles responsible for the VLF hiss emissions.

II. INSTRUMENTATION

The data used in this study were obtained from the NASA/University of Iowa satellite Injun 5. This satellite was launched on August 8, 1968, into an elliptical polar orbit with an inclination of 80.66°, an apogee altitude of 2528 km, and a perigee altitude of 677 km. The satellite carries a tape recorder with a bit rate of 800 bits $(\text{second})^{-1}$ to provide world-wide spatial surveys and a high bit rate mode of operation at 24,000 bits $(\text{second})^{-1}$ to provide high temporal resolution measurements of auroral phenomena. The spacecraft is magnetically oriented by a bar magnet within the spacecraft.

The VLF instrumentation on Injun 5 consists of one electric dipole antenna, one magnetic loop antenna, two wide-band (30 Hz to 10 kHz) receivers, and a six channel step-frequency receiver covering the frequency range from 7.5 kHz to 105 kHz. The electric and magnetic antennas are mounted in such a way that the Poynting flux direction of the VLF waves, up or down the geomagnetic field, can be determined from the correlation between the electric and magnetic field signals. A complete description of the Injun 5 VLF instrumentation is given by Gurnett *et al.*, [1969].

Simultaneous measurements of electron and proton intensities within the energy range $5 \leq E \leq 50{,}000$ eV are obtained from two Low-Energy Proton and Electron Differential Energy Analyzers (abbreviated, LEPEDEA'S) on Injun 5, one (LEPEDEA 'A') with a field of view directed anti-parallel to the local geomagnetic field vector and the other (LEPEDEA 'B') with a field of view directed perpendicular to the local geomagnetic field vector. Hence LEPEDEA 'A' measures the precipitated fluxes into the earth's atmosphere over the Northern hemisphere and the upgoing fluxes over the Southern hemisphere. Energetic electron intensities with energies $E > 45$ keV are surveyed with a companion set of collimated, thin-windowed Geiger-Mueller tubes. Further details of this charged particle instrumentation are given by Frank and Ackerson [1971].

III. OBSERVATIONS

A. Survey of VLF Hiss and Associated Plasma Observations

In order to identify the magnetospheric plasma regime involved in the generation of auroral zone VLF hiss, a global survey of the VLF/LEPEDEA data was performed using the tape recorded data. For the data presented in this portion of the study, the LEPEDEA instrumentation was operated in a special 'survey' mode of operation. This mode of operation provided a high sensitivity over a wide energy range and is particularly suitable for identifying the various plasma regimes in the distant magnetosphere, e.g., polar cap, polar cusp, plasma sheet, and proton ring current. A total of ten orbits, selected to provide a coarse sampling of all local times, has been analyzed in detail. From these data, five polar passes have been selected for presentation in Figures 1 through 5 as representative of the VLF hiss and associated charged particle fluxes observed.

Figure 1 illustrates an example of an auroral zone VLF hiss event observed during a polar pass over the northern hemisphere near the noon-midnight meridional plane. The VLF electric field spectral densities observed on this pass are shown on the top panel of Figure 1 at three

representative frequencies: 7.35 kHz, 22 kHz, and 70 kHz. A broad-band VLF noise emission, characteristic of auroral zone VLF hiss, occurs on this pass from approximately 15:11:30 to 15:13:30 UT. The VLF hiss spectrum in this case extends from below 7.35 kHz to above 105 kHz, the highest frequency measured, and the integrated broad-band electric field strength is about 3 mV $(\text{meter})^{-1}$. The magnetic local time (MLT) and invariant latitude (INV) at the time of maximum intensity for this event are about 10.2 hours and 76°, respectively.

During the time when the VLF hiss is observed, the DC electric field data for this pass show a negative perturbation in the measured DC electric field of about 30 mV $(\text{meter})^{-1}$ from the $\vec{V}_s \times \vec{B}$ electric field caused by the satellite motion through the ionosphere. This electric field perturbation corresponds to a westward (anti-sunward) plasma convection of about 1 km $(\text{sec})^{-1}$ [see Cauffman and Gurnett, 1971, for a discussion of the Injun 5 DC electric field experiment and its interpretation].

As shown by the $325 \leq E \leq 570$ eV electron and $290 \leq E \leq 455$ eV proton intensities in Figure 1, the VLF hiss event on this pass occurs in a region of very intense, low-energy (several hundred eV) electron and proton fluxes on the poleward side of the electron $E > 45$ keV trapping boundary. The charged particle fluxes in this region consist

of an equatorward 'electron sheet' and an adjacent poleward 'proton sheet' shown shaded in Figure 1. Frank [1971a] has recently reported observations of similar proton and electron sheets at high altitudes, ~ 5 R_E, in the dayside polar magnetosphere with the eccentric orbiting satellite IMP-5. The widths of each sheet of $\sim 2°$, the proton and electron intensities and the relative juxtaposition of these two sheets at low altitudes as shown in Figure 1, are in substantial agreement with the IMP-5 results. These two sheets are identified with the direct entry of magnetosheath plasma into the dayside polar magnetosphere. The corresponding region of direct access of magnetosheath plasma is called the polar cusp [Frank, 1971a]. Similar low-altitude observations of magnetosheath plasma during local day have been previously reported by Frank and Ackerson [1971]. Heikkila and Winningham [1971] have also presented detailed observations of this phenomena at low-altitudes for a selected pass during very distrubed magnetic conditions ($K_p = 6$; $\Sigma K_p = 41$, $A_p = 54$). The polar cusp observations of Figure 1 are, however, unusual in that (1) the separation of the polar cusp plasma into distinct proton and electron sheets, commonly observed at high altitudes, is not usually found at low altitudes, and (2) the proton intensities are more intense than usual. On the other hand, this series of observations provides us with a convincing identification of

the position of the low-altitude intersection of the polar cusp relative to the various phenomena (e.g., trapping boundary, VLF hiss, plasma convection, etc.) at Injun 5 altitudes.

The very soft energy spectrum of the polar cusp electrons is illustrated in the bottom panel of Figure 1 by the very low (background level) flux of $1160 \leq E \leq 2040$ eV electrons in the polar cusp region and over the entire polar cap region. The abrupt increase in the $1160 \leq E \leq 2040$ eV electron flux at 15:13:45 UT marks the transition from the polar cusp region to the outer radiation zone and is coincident with the trapping boundary for electrons with energies $E > 45$ keV.

From the charged particle intensities shown in Figure 1, it is evident that the VLF hiss observed on this pass is closely associated with the low energy polar cusp plasma. No significant VLF hiss emission is observed in the outer radiation zone which is characterized by much higher electron energies, or in the polar cap region which is essentially void of charged particles with energies $E \gtrsim 50$ eV.

Figures 2 and 3 illustrate two successive polar passes over the <u>southern</u> hemisphere for morning-evening (08:00-20:00) local times. During the first pass, shown in Figure 2, a very weak VLF hiss event is observed in the local evening ($\sim$21.0 hr. MLT), from about 15:36 to 15:37 UT, and

a much more intense event is observed in the local morning (~0800 MLT), from about 15:46 to 15:49 UT. On the succeeding pass two hours later, shown in Figure 3, the intensity of the VLF hiss has increased considerably in the local evening, from 17:37 to 17:40 UT, and is about the same in the local morning, from 17:46 to 17:49 UT.

From the corresponding charged particle intensities shown in Figures 2 and 3, it is evident that the VLF hiss occurs in regions with intense fluxes, $>10^5$ electrons $(cm^2\text{-sec-sr-eV})^{-1}$, of low-energy electrons with energies on the order of one to several hundred eV. In the local morning region, these low-energy electrons are again identified by their soft energy spectrum as having originated from the magnetosheath/polar cusp region. This identification is further supported by the observation of an enhanced flux of $290 \leq E \leq 455$ eV protons from 17:47 to 17:49 UT in Figure 3 with energy spectra typical of magnetosheath protons. In contrast to the large polar cusp proton fluxes, $>10^5$ protons $(cm^2\text{-sec-sr-eV})^{-1}$, observed for the pass in Figure 1, the polar cusp proton fluxes observed in Figure 3, $\lesssim 10^4$ protons $(cm^2\text{-sec-sr-eV})^{-1}$, are more typical. It is further noted that the proton intensities in the VLF hiss region are quite small, at ~17:38 UT in Figure 3, for example, thereby identifying the low-energy electrons as the particles responsible for the VLF hiss emission.

The correlation between the occurrence of VLF hiss and the low-energy (few hundred eV) electrons is particularly evident for the local evening auroral zone crossings in Figures 2 and 3. During the local evening portion of the pass in Figure 2, both the low energy electron fluxes and the VLF hiss intensities are small. On the following orbit, however, the low energy electron flux ($160 \leq E \leq 280$ eV, in particular) increases by about two orders of magnitude and the broad-band VLF hiss intensity increases accordingly.

In the local evening, the intense fluxes of low-energy electrons observed on the poleward side of the electron $E > 45$ keV trapping boundary, such as from 17:37 to 17:40 UT in Figure 3, are identified with magnetosheath electron intensities which have been energized by an auroral acceleration process at altitudes $\lesssim 5\ R_E$ [Frank and Gurnett, 1971; Frank and Ackerson, 1971]. Further examples of these energetic auroral electron events will be presented and discussed in the following section on high-time resolution observations.

For the southern hemisphere observations of Figures 2 and 3, LEPEDEA 'A', which detects particles with pitch angles of $\alpha = 0°$, is detecting the flux of charged particles coming up the geomagnetic field from below the

satellite. For these passes, the upgoing ($\alpha = 0°$) electron flux is usually less than, or comparable to, the flux perpendicular ($\alpha = 90°$) to the geomagnetic field. Generally these upgoing electron fluxes can be attributed to backscattering of precipitated electrons from the atmosphere below the satellite. However, near the trapping boundary at 17:49:30 UT in Figure 3, an intense flux of upgoing $110 \leq E \leq 190$ eV electrons is observed. For this event, the ratio of the upgoing, $\alpha = 0°$, to the perpendicular, $\alpha = 90°$, flux is about 3:1. At higher energies, several hundred eV and above, this anisotropy of electron intensities is not observed. Similar upgoing electron events of this type, sometimes with anisotropy ratios as large as 100:1, are frequently observed with Injun 5.

Figures 4 and 5 illustrate two further examples of auroral zone VLF hiss and the relevant charged particle data for successive northern and southern hemisphere passes at approximately 5.0 and 17.0 hr. local times. These passes show a marked asymmetry between dawn and dusk local times with VLF hiss occurring at roughly magnetically conjugate locations in the dusk local time regions. Again the VLF hiss is observed on the poleward side of the electron $E > 45$ keV trapping boundary, and in regions with intense fluxes of electrons with energies on the order of a few

hundred eV. For the southern hemisphere data in Figure 5 intense anisotropic fluxes of upgoing $155 \leq E \leq 275$ eV electrons are evident at 15:43:45 and 15:45:50 UT. The measurements of electron intensities at $\alpha = 0°$ ($155 \leq E \leq 275$ eV) and 90° ($160 \leq E \leq 280$ eV) are simultaneous. The ratio of the upgoing ($\alpha = 0°$) to the perpendicular ($\alpha = 90°$) flux for the event at 14:45:50 UT is approximately 100:1.

B. High-Temporal Resolution Observations

In this section, observations from several high bit rate passes over the auroral zone are presented to illustrate the detailed spatial and temporal structure of VLF hiss and related phenomena. For this portion of the study, a total of about twenty high bit rate passes has been investigated at various local times to determine the details of the charged particle/VLF relationships. The passes selected for presentation have been chosen to illustrate a variety of effects observed.

Observations Near Local Noon. Figure 6 shows an energy-time spectrogram of the precipitated electron flux observed for a high bit rate pass through the polar cusp region at about 10.2 hours magnetic local time. On this pass the trapping boundary for electrons $E > 45$ keV occurred at about 23:30:50 UT. At latitudes equatorward of the trapping boundary, the electron energy spectrum is relatively

hard with energies (1-10 keV) typical of the outer radiation zone at these local times [Frank and Ackerson, 1971]. Near the trapping boundary at about 23:31:00 UT, a brief (4 second) intense flux, $\sim 10^9$ electrons $(cm^2\text{-sec-sr})^{-1}$, of low-energy ($\sim$100 eV) electrons is observed. These low-energy electrons continue to be observed with reduced intensities, $\sim 3 \times 10^7$ electrons $(cm^2\text{-sec-sr})^{-1}$, until, at approximately 23:32:10 UT, the flux abruptly decreases to a low level typical of the polar cap region. On the basis of their energy spectra, intensities, angular distributions, and location relative to the trapping boundary and polar-cap region, these low-energy electrons are identified as having originated from the dayside magnetosheath and the corresponding region, from 23:31:00 to 23:32:10 UT, is identified as the polar cusp.

Further evidence of the polar cusp location in this case is provided by the DC electric field data shown in Figure 7. The sinusoidal variation of the measured electric field with a period of about 8 minutes is caused by the satellite rotation in the $\vec{V}_s \times \vec{B}$ field. A 50 to 100 mV/meter perturbation of the measured electric field from the $\vec{V}_s \times \vec{B}$ field is observed from 23:31:00 to 23:32:00 UT, in almost exact correspondence with the polar cusp region identified with the charged particle data. This electric field corresponds to an <u>eastward</u> plasma convection of about

1.5 to 3.0 km/sec. This convection direction is in contrast to the westward convection direction observed for the pass in Figure 4. Eastward convection indicates that in this case the 'stagnation point' for the east-west plasma flow in the polar cusp region is on the dawn side of the magnetosphere at a magnetic local time less than 10.2 hr. For further details on high-latitude plasma convection observations with Injun 5, the reader is referred to Cauffman and Gurnett [1971].

The frequency-time spectra of the VLF electric and magnetic fields observed during this pass are shown in Figure 8. In the outer radiation zone region, at latitudes equatorward of the trapping boundary for electrons $E > 45$ keV, the primary VLF noise observed is chorus and ELF hiss. At the trapping boundary the chorus and ELF hiss emissions disappear and the spectrum changes abruptly to VLF hiss with impulsive temporal structure characteristic of VLF hiss near local noon [Gurnett, 1966]. The region of maximum intensity for the auroral hiss emission corresponds well with the polar cusp region identified from the charged particle and convection electric field data. The maximum broad-band (300 Hz to 10 kHz) VLF electric and magnetic field intensities in this case are approximately 0.53 mV $(\text{meter})^{-1}$ and 1.8 milligammas, respectively. The increased intensity of the electric field spectra compared to the magnetic field spectra, evident in Figure 8, is mainly

attributed to the greater sensitivity of the Injun 5 electric antenna compared to that of the magnetic antenna.

Observations Near Local Evening. The charged particle and VLF data observed for a high bit rate pass over the northern auroral zone in the local evening at approximately 22.0 hr. magnetic local time are shown in Figures 9 and 10. During this pass, a moderately intense auroral electron precipitation event occurred from about 04:05:20 to 04:06:20 UT as shown by the LEPEDEA 'A' energy-time spectrogram in Figure 9. This event was characterized by relatively low electron energies, primarily less than 1 keV, and maximum electron fluxes of about 2×10^9 electrons $(cm^2\text{-sec-sr})^{-1}$. On this pass the electron E > 45 keV trapping boundary occurred at about 04:06:20 UT, coincident with the equatorward boundary of the electron precipitation region.

Using the correlation techniques described by Gurnett et al., [1971] the VLF electric and magnetic field signals for this pass have been processed to give separate frequency-spectrograms of waves propagating up and down the geomagnetic field as shown in Figure 10. From these spectrograms it is evident that two distinct types of VLF noise occurred in association with the electron precipitation event shown in Figure 9. On the downgoing spectrogram, a VLF hiss event is observed with a frequency spectrum more or less typical of VLF hiss observed in the local evening [Gurnett, 1966].

The temporal/spatial location of this auroral zone VLF hiss event corresponds almost exactly (±10 seconds) with the region of maximum electron precipitation shown in Figure 9.

The power flux of the VLF hiss in this event can be estimated using the Poynting flux measurement theory of Mosier and Gurnett [1971]. For the Injun 5 antenna configuration it can be shown that the correlation, $\langle E_x H_y \rangle$, between the electric, E_x, and magnetic, H_y, field signals is proportional to the average Poynting flux component, $\langle S_z \rangle$, parallel to the geomagnetic field, $\langle E_x H_y \rangle = G(\vec{K}) \langle S_z \rangle$. The proportionality factor $G(\vec{K})$ is a function of the wave normal direction and is not known precisely since the wave normal direction is generally unknown. It can be shown, however, that $G(\vec{K})$ is always positive and less than 1 at VLF frequencies and that the average value of $G(\vec{K})$, averaged over all wave directions, is 1/2. We can therefore place a lower limit on the Poynting flux of $\langle S_z \rangle \geq \langle E_x H_y \rangle$ and make a best estimate for the Poynting flux of $\langle S_z \rangle \simeq 2 \langle E_x H_y \rangle$. The correlation $\langle E_x H_y \rangle = |E_x||H_y| \langle \cos \phi \rangle$ is determined most accurately from the Injun 5 telemetry by using the on-board electric and magnetic field strength measurements, $|E_x|$ and $|H_y|$, and by measuring the average value of the cosine of the phase angle between the electric and magnetic field signals, $\langle \cos \phi \rangle$, from the wide band telemetry.

For the VLF hiss event shown in Figure 9 the broad-band, 300 Hz to 10 kHz, electric and magnetic field strengths at the time of maximum intensity (04:05:48 UT) are 1.67 mV(meter)$^{-1}$ and 11.4 milligammas, respectively, and the cosine correlation $\langle \cos \phi \rangle$, is approximately 0.7. Using an effective noise bandwidth for the emission of 5 kHz, the corresponding lower limit on the VLF power flux for this event is 2.0×10^{-12} watts (meter^2-Hz)$^{-1}$. The actual power flux is larger, probably on the order of 4.0×10^{-12} watts (meter^2-Hz)$^{-1}$.

On the upgoing spectrogram shown in Figure 10, a VLF emission called a saucer is observed. Saucers are characterized by a parabola shaped appearance on a frequency time spectrogram, typically with a duration of about 10 seconds or less, and are invariably observed to be propagating up the geomagnetic field from below the satellite [Mosier and Gurnett, 1969]. In contrast to the downgoing VLF hiss, the saucer is <u>not</u> located in the region of maximum electron precipitation, but rather is located at the equatorward boundary of the electron precipitation event and near the electron E > 45 keV trapping boundary. This relationship is typical of most saucers observed with Injun 5 in that saucers do not normally occur in the region of most intense electron precipitation, but rather occur at the boundary of a precipitation band. Saucers have been observed in situations where no downgoing electron or proton fluxes,

E > 50 eV, above the background level of the LEPEDEA instrumentation and with an appropriate duration, 10 seconds, could be associated with the saucer emissions. Unfortunately, because of limitations on receiving the high bit rate and broad-band VLF telemetry no suitable data are available from the southern hemisphere, where LEPEDEA 'A' views particles coming up the geomagnetic field from the ionosphere, to investigate the possibility that saucers may be caused by upgoing electrons. The possibility that saucers may be associated with upgoing low-energy electrons is considered further in the interpretation and discussion section of this paper.

The charged particle and VLF data observed during another pass at about 19.0 hr. magnetic local time in the local evening are shown in Figures 11 and 12. The low-energy electron precipitation region observed with LEPEDEA 'A' during this pass is very broad extending from approximately 22:54:15 to 22:56:50 UT. The electron energy-time spectrogram for this pass shows a series of inverted 'V' structures of the type identified by Frank and Ackerson [1971]. The average electron energy in these inverted 'V' events extends to several keV and the maximum electron fluxes are about 1.6×10^{9} electrons $(cm^{2}\text{-sec-sr})^{-1}$. The electron E > 45 keV trapping boundary occurs near the end of the pass at 22:57:50 UT equatorward of the intense low-energy electron

precipitation. A detailed discussion of this series of observations and representative spectra are given in the survey by Frank and Ackerson [1971].

The VLF frequency-time spectrograms for this pass again show distinctly different phenomena on the upgoing and downgoing spectrograms. On the downgoing spectrogram the most prominent VLF noise phenomena observed are the two V-shaped VLF hiss events at about 22:55:10 and 22:56:00 UT. V-shaped VLF hiss events of this type have been previously discussed by Gurnett [1966] and are the most common spectral form of VLF hiss observed during local evening. V-shaped VLF hiss events can be distinguished from saucers on the basis of their duration which, for the Injun 5 orbit, is typically about 1 minute (or 500 km latitudinal width). The broad-band electric and magnetic field strengths observed for the first V-shaped hiss event at 22:55:10 UT are about 4.2 mV(meter)$^{-1}$ and 10.0 milligammas, respectively, and the cosine correlation, $\langle \cos \phi \rangle$, is about 0.5. The corresponding VLF power flux for this event is at least 5.5×10^{-12} watt (meter^2 Hz)$^{-1}$, and probably about 1.1×10^{-11} watt (meter^2 Hz)$^{-1}$. From the charged particle and VLF spectrograms in Figures 11 and 12, it is evident that the downgoing V-shaped VLF hiss events occur in the same region as the inverted 'V' electron precipitation events. The

similarity in the duration and relative locations of the V-shaped hiss events and the inverted 'V' electron precipitation events shows that these phenomena are closely related. In general, for this and other similar cases, the detailed temporal (or spatial) features of these two phenomena are not always coincident on time (or distance) scales of less than about 10 seconds (100 km). However, since the VLF hiss is probably generated well above the Injun 5 altitude and the VLF ray paths do not necessarily follow the charged particle trajectories, this lack of a detailed correspondence in all cases is not surprising.

On the upgoing spectrogram in Figure 12 a saucer is observed at approximately 22:58:00 UT. Again the upgoing saucer emission is observed near the boundary of the primary electron precipitation region and no clearly identifiable feature in the precipitated electron spectrum with a time scale comparable to, or less than, the saucer duration can be associated with the saucer.

IV. SUMMARY OF OBSERVATIONS

A variety of examples of auroral zone VLF hiss and related plasma phenomena in the polar magnetosphere has been presented. On the basis of these and other cases investigated but not presented here, we summarize below the principal observational results of this study.

(1) Auroral zone VLF hiss is observed near and on the poleward side of the 'trapping boundary' for energetic electrons E > 45 keV in a zone typically about 7° wide in latitude centered on 77° INV at local noon decreasing to 72.0° INV at local midnight. The electron E > 45 keV trapping boundary is observationally identified with the high-latitude termination of measurable electron E > 45 keV intensities.

(2) In this region near and poleward of the electron E > 45 keV trapping boundary, VLF hiss is associated with intense fluxes of precipitating low-energy electrons with energies on the order of one hundred eV to several keV. On the dayside of the magnetosphere, the region where these low-energy electron fluxes and the

associated VLF hiss are observed is identified as the dayside polar cusp. On the nightside of the magnetosphere, the corresponding region of occurrence of VLF hiss is identified with the downstream magnetosheath and the distant plasma sheet which are the topological extensions of the polar cusp into the magnetotail.

(3) A pronounced day-night asymmetry exists in the occurrence and spectral character of both the VLF hiss and the associated low energy electron flux [cf. Figures 1 through 5 and Figures 8 and 10]. During the local day detectable levels of VLF hiss and low-energy electron fluxes are essentially omnipresent in the polar cusp region. The electron energy spectrum in the dayside polar cusp is normally very soft ($\sim$100 eV) and shows relatively little evidence of acceleration or heating of the magnetosheath electrons. The VLF hiss frequency-time spectrum in the dayside polar cusp is characterized by rapid temporal variations of all frequencies on a time scale of a few seconds [cf. Figure 8] and is called impulsive VLF hiss by Gurnett [1966]. During the local evening the VLF hiss intensities

and the low energy electron intensities are highly variable [cf. Figures 2 and 3]. The electron energy spectrum in the local evening is characterized by inverted 'V' precipitation events and shows considerable evidence of acceleration and heating. The VLF hiss spectrum in the local evening often shows a V-shaped frequency-time structure [cf. Figure 12]. In many cases where multiple inverted 'V' events occur, there appears to be a close correspondence between individual inverted 'V' events and the V-shaped VLF hiss events.

(4) There is evidence of a significant dawn-dusk asymmetry in the occurrence of VLF hiss and the spectral characteristics of the precipitated electrons. In particular, in the early morning region from 0.0 to 6.0 hours local time, both VLF hiss and the inverted 'V' electron precipitation events are relatively uncommon.

(5) VLF hiss is generally observed to be propagating down the geomagnetic field from a generation region above the spacecraft. The power flux of VLF hiss is sometimes as large as 10^{-12} to 10^{-11} watt $(\text{meter}^2\text{-Hz})^{-1}$. The corresponding energetic charged particle fluxes observed for the VLF

hiss events of this intensity have energies on the order of 100 eV to several keV and fluxes of about 10^9 electrons $(cm^2\text{-sec-sr})^{-1}$ [see for example, the discussion of Figures 9 and 11].

(6) Some evidence exists indicating that there is a 'threshold' low-energy electron flux below which VLF hiss is not observed. A cursory examination of Figures 1 through 5, as well as other examples investigated but not shown, indicates that when the ∿100 eV electron flux is less than about 10^4 to 10^5 electrons $(cm^2\text{-sec-sr-ev})^{-1}$ there is little or no VLF hiss present. When the low-energy electron flux is above this 'threshold' VLF hiss is essentially always observed, however the VLF hiss intensity is not necessarily proportional to the low-energy charged particle flux [cf. Figures 1 and 4].

(7) Intense highly anisotropic fluxes of upgoing low-energy (∿100 eV) electrons, $j(\alpha = 0°)/j(\alpha = 90°) >> 1$, are frequently observed in the VLF hiss region. These upgoing low-energy electrons occur in a very narrow zone, less than ∿2° in latitudinal width, usually comprising only one measurement (1 minute time resolution) in the low bit rate tape recorded data [cf.

Figure 5]. The absence of high bit rate telemetry coverage in the southern hemisphere, where LEPEDEA 'A' views upcoming particles, prevents us from investigating these events with higher time resolution in this study. However, an analysis of high bit rate data during the period immediately following launch for which the spacecraft was spinning before magnetic stabilization occurred is currently being undertaken and should yield more information concerning the upgoing electron fluxes.

(8) Near the boundary of the low-energy electron precipitation regions associated with the downgoing VLF hiss, a type of VLF radio noise called a saucer is often observed propagating up the geomagnetic field from a generation region below the satellite. These saucer emissions are always of short duration, typically 10 seconds or less, and are suggestive of a very narrow ($\sim$100 km) latitudinal source width. In no case has it been possible to associate a charged particle precipitation event ($E > 50$ eV) of corresponding duration as, and simultaneous with, a saucer. Although it is considered likely that the saucer emissions are associated with the upgoing

electrons discussed earlier, this relationship cannot be confirmed because of the limited broad-band VLF data available from the southern hemisphere, where these upgoing electron fluxes can be detected.

V. DISCUSSION AND INTERPRETATION

The results of this study provide the first direct verification of the association between auroral zone VLF hiss and intense fluxes, 10^4 to 10^7 electrons $(cm^2\text{-sec-sr-eV})^{-1}$, of low energy electrons with energies on the order of 100 eV to several keV. On the dayside of the magnetosphere, these low-energy electrons are identified with the dayside polar cusp region observed by Frank [1971a] at higher altitudes with the IMP-5 satellite. At other local times, through the dawn and dusk regions and into the nightside of the magnetosphere, the VLF hiss and associated low-energy electron precipitation regions are believed to correspond to the longitudinal extension of the dayside polar cusp plasma into the distant plasma sheet and downstream magnetosheath on the nightside of the magnetosphere, following the observational model of Frank [1971b]. As discussed by Frank [1971a, b], the magnetic field lines throughout this region of low-energy electron precipitation are 'open', thereby providing for the direct entry of magnetosheath plasma. Low-altitude observations by Frank and Gurnett [1971] show that this region is also characterized by anti-solar plasma flow reflecting the bulk motion of

magnetosheath plasma past the earth. On the nightside of the magnetosphere significant acceleration of the magnetosheath electrons is observed, as characterized by the inverted 'V' electron precipitation events. As discussed by Frank and Gurnett [1971] the character of these electron precipitation events suggests that the electron acceleration is caused by quasi-static electric fields parallel to the geomagnetic field at altitudes $\lesssim 5R_E$.

The observation of a significant energy spread for the electron spectra within these inverted 'V' precipitation bands, sometimes comparable to the average energy of the electron spectra, indicates that considerable heating or scattering of the precipitated electron beam must occur if the primary acceleration process is due to quasi-static electric fields. The association of intense VLF hiss with inverted 'V' electron precipitation events suggests that VLF hiss may be closely related to this heating process. A variety of instability mechanisms is known which could cause the observed heating and VLF hiss generation (see, for example, Kindel and Kennel [1971]). The absence of any detectable <u>precipitating</u> charged particle flux, E > 50 eV, with a latitudinal width (<10 km) suitable for explaining the saucer emissions, and the correspondingly narrow latitudinal width and region of occurrence of the saucer emissions and the intense fluxes of upgoing low-energy electrons commonly

observed near the inverted 'V' electron precipitation regions, provide us with some evidence that saucers are generated by these upgoing electrons.

The generation of VLF hiss by incoherent Cerenkov radiation, as proposed by Jørgensen [1968], Hartz [1971], and others, is considered unlikely as a general process for explaining VLF hiss because of the large power fluxes sometimes observed. This difficulty with the incoherent Cerenkov radiation mechanism is illustrated, for example, by the event in Figures 11 and 12, which has an electron energy spectrum at the peak of the inverted 'V' very similar to that used by Jørgensen [1968] for a calculation of the VLF power flux due to Cerenkov radiation. The power flux of the VLF hiss in this event is observed to be greater than 5×10^{-12} watt $(m^2\text{-Hz})^{-1}$, whereas Jørgensen's model calculations indicate a maximum power flux of about 10^{-14} watt $(m^2\text{-Hz})^{-1}$, thus leaving a discrepancy of about a factor of 500 between the computed and observed power fluxes. Similar conclusions are obtained for the event in Figures 9 and 10 after corrections are included for the lower average electron energies and increased Cerenkov radiation expected in this case. These intense events, although probably not representative of the 'average' intensity of a VLF hiss event, serve to illustrate the difficulties of explaining all the observed VLF hiss emissions by an incoherent radiation process. The aforementioned evidence of a threshold electron flux necessary

for the generation of VLF hiss appears to be also indicative of a coherent plasma instability, and not an incoherent process, operative in some, if not all, of these events.

The configuration envisioned for the generation of VLF hiss and saucer emissions is illustrated in Figure 13. This model is intended to explain the main observational features of local evening events similar to those shown in Figures 10 and 12. In this model, downgoing VLF "auroral hiss" is generated at an altitude above the satellite by downgoing magnetosheath electrons which have been accelerated to form an inverted 'V' electron precipitation event. At a lower latitude, near or at the boundary between 'open' and 'closed' field lines, an upgoing saucer emission is generated below the satellite by the upgoing ionospheric electron flux which forms the return current. That such a field aligned current configuration does occur can only be inferred indirectly from the Injun 5 measurements; however, Cloutier et al., [1970] have observed an essentially identical current configuration with rocket-borne magnetometers over an auroral arc in the local evening. Although the detailed generation mechanism for the saucer is not known, the frequency-time shape of the saucer can be explained in some detail by the frequency dependence of the limiting ray angle for whistler mode propagation from the generation region to

the satellite [Mosier and Gurnett, 1969]. From the frequency-time envelope of a saucer, Mosier and Gurnett have estimated the source location for a representative saucer to be about 1100 km below the satellite and at an altitude of about 1400 km. The general similarity in the spectral form of saucers and V-shaped VLF hiss events suggests that the V-shaped form of the VLF hiss observed in the local evening is also caused by the same limiting ray angle effect for downgoing whistler mode waves. If this is the case, then a coarse estimate for the height of the VLF hiss generation region above the satellite is given by 1100 km x (latitudinal width of a V-shaped VLF hiss event/latitudinal width of a saucer). This rough estimate typically places the VLF hiss generation region at an altitude of about 5,000 to 10,000 km. If the VLF hiss is associated with the heating of the precipitated electrons, it is suggestive that this may also be the altitude where the primary auroral acceleration process occurs.

ACKNOWLEDGMENTS

This research was supported in part by the National Aeronautics and Space Administration under contracts NAS5-10625, NAS1-8141, NAS1-8144(f), NAS1-8150(f), and grant NGL-16-001-043(7), and by the Office of Naval Research under contract N00014-68-A-0196-0003.

REFERENCES

Cauffman, D. P. and D. A. Gurnett, Double probe measurements of DC electric fields with the Injun 5 satellite, J. Geophys. Res., (submitted for publication), 1971

Cloutier, P. A., H. R. Anderson, R. J. Park, R. R. Vondrak, R. J. Spiger, and B. R. Sandel, Detection of geomagnetically aligned currents associated with an auroral arc, J. Geophys. Res., 75, 2595, 1970.

Eather, R. H. and S. B. Mende, Airborne observations of auroral precipitation patterns, J. Geophys. Res., 7, 1746, 1971.

Ellis, G. R. A., Low frequency electromagnetic radiation associated with magnetic disturbances, Planetary Space Sci., 1, 253, 1959.

Frank, L. A., Plasma in the earth's polar magnetosphere, J. Geophys. Res., (submitted for publication), 1971a.

Frank, L. A., Comments on a proposed magnetospheric model, J. Geophys. Res., 76, 2512, 1971b.

Frank, L. A., and K. L. Ackerson, Observations of charged particles precipitated into the auroral zone, J. Geophys. Res., (submitted for publication), 1971.

Frank, L. A. and D. A. Gurnett, On the distribution of plasmas and electric fields over the auroral zones and polar caps, J. Geophys. Res., (submitted for publication), 1971.

Gurnett, D. A., A satellite study of VLF hiss, J. Geophys. Res., 71, 5599, 1966.

Gurnett, D. A., S. R. Mosier, and R. R. Anderson, Color spectrograms of very-low-frequency Poynting flux data, J. Geophys. Res., 76, 3022, 1971.

Gurnett, D. A., G. W. Pfeiffer, R. R. Anderson, S. R. Mosier, and D. P. Cauffman, Initial observations of VLF electric and magnetic fields with the Injun 5 satellite, J. Geophys. Res., 74, 4631, 1969.

Hartz, T. R., Particle precipitation patterns, Aurora and Airglow, 1970, B. M. McCormac, ed., Van Nostrand Reinhold Co., New York, 1971 (in press).

Heikkila, W. J., and J. D. Winningham, Penetration of magnetosheath plasma to low altitudes through the dayside magnetospheric cusps, J. Geophys. Res., 76, 883, 1971.

Helliwell, R. A., Whistlers and Related Ionospheric Phenomena, Stanford University Press, Stanford, California, 1965.

Johnson, R. G., and R. D. Sharp, Satellite measurements on auroral particle fluxes, Atmospheric Emissions, B. M. McCormac and A. Omholt, eds., Van Nostrand Reinhold Co., 1969.

Jørgensen, T. S., Interpretation of auroral hiss measured on OGO 2 and at Byrd Station in terms of incoherent Cerenkov radiation, J. Geophys. Res., 73, 1055, 1968.

Kindel, J. M., and C. F. Kennel, Topside current instabilities, J. Geophys. Res., 76, 3055, 1971.

Laaspere, T., W. C. Johnson, and L. C. Semprebon, Observations of auroral hiss, LHR noise, and other phenomena in the frequency range 20 Hz - 540 kHz on OGO 6, J. Geophys. Res., (submitted for publication), 1971.

McEwen, D. J. and R. E. Barrington, Some characteristics of the lower hybrid resonance noise bands observed by the Alouette 1 satellite, Can. J. Phys., 45, 13, 1967.

Mosier, S. R. and D. A. Gurnett, VLF measurements of the Poynting flux along the geomagnetic field with the Injun 5 satellite, J. Geophys. Res., 74, 5675, 1969.

Mosier, S. R. and D. A. Gurnett, Theory of the Injun 5 very-low-frequency Poynting flux measurements, J. Geophys. Res., 76, 972, 1971.

FIGURE CAPTIONS

Figure 1 Simultaneous observations of VLF hiss, convection electric fields, and charged particle fluxes for a noon-midnight meridional pass over the northern auroral zone and polar cap region. This pass provides a clear demonstration of the association between the polar cusp plasma and auroral zone VLF hiss and illustrates the relative locations of the VLF hiss region, the polar cusp plasma convection, the polar cusp electron and proton sheets, and the electron E > 45 keV trapping boundary. ($Kp=2^-$.)

Figure 2 Simultaneous observations of VLF hiss and intense fluxes of several hundred eV electrons for a morning-evening (08:00 - 21:00 MLT) pass over the southern hemisphere. Note the low electron fluxes for the 21:00 MLT auroral zone crossing and the corresponding low VLF hiss intensities. ($Kp=1^-$.)

Figure 3 Continuation of Figure 2 for the following southern hemisphere pass approximately two hours later. Note the greatly increased flux of low-energy, several hundred eV, electrons for the 21:00 MLT auroral zone crossing compared to Figure 2 and the corresponding increase in the VLF hiss intensity. An intense flux of upgoing ($\alpha = 0°$), $110 \leq E \leq 190$ eV, electrons is observed near the trapping boundary at 17:49:30 UT.

Figure 4 Observations of VLF hiss and associated low-energy electron fluxes for a dawn-dusk (05:00-17:00 MLT) pass over the northern hemisphere. Note the asymmetry between dawn and dusk local times. Inverted 'V' electron precipitation bands centered at ∿14:43 and 14:53 U.T. have been previously identified by Frank and Gurnett [1971]. The precipitation band at local morning is unusual in the fact that the fluxes of low-energy electrons E > 50 eV were $\sim 10^8$ $(cm^2\text{-sec-sr})^{-1}$, approximately a factor of 10 less than is typically observed in these events. ($Kp=3^-$.)

Figure 5 Continuation of Figure 4 for the following southern hemisphere pass approximately one hour later. ($Kp=2^{+}$.)

Figure 6 LEPEDEA 'A' energy-time spectrogram for a northern hemisphere pass through the polar cusp region near local noon (10:00 MLT). The electron $E > 45$ keV trapping boundary is located at about 23:30:50 UT and the region from 23:31:00 to 23:32:10 UT is identified as the polar cusp. ($Kp=3$.)

Figure 7 DC electric field observations for the polar cusp crossing in Figure 6. The $\vec{V}_s \times \vec{B}$ field is caused by the spacecraft motion through the ionosphere. The electric field perturbation from the $\vec{V}_s \times \vec{B}$ field, from 23:31:00 to 23:32:00 UT, corresponds to an eastward plasma convection in the polar cusp region.

Figure 8 VLF electric and magnetic frequency-time spectrograms for the polar cusp crossing in Figure 6 showing the occurrence of chorus and ELF hiss equatorwards of the $E > 45$ keV trapping boundary and VLF hiss in the polar cusp region.

Figure 9 LEPEDEA 'A' energy-time spectrogram of an intense, 2 x 10^9 electrons $(cm^2\text{-sec-sr})^{-1}$, low-energy, $E \lesssim 1$ keV, electron precipitation event in the local evening (22:00 MLT). The electron E > 45 keV trapping boundary is at 04:06:20 UT. ($Kp=0^+$.)

Figure 10 Frequency-time spectrograms showing downgoing VLF hiss and an upgoing saucer emission associated with the low energy electron precipitation event in Figure 9. Note that the VLF hiss occurs in the region of most intense electron flux, whereas the saucer occurs at the equatorward boundary of the precipitation region and near the electron E > 45 keV trapping boundary.

Figure 11 LEPEDEA 'A' energy-time spectrogram showing a series of inverted 'V' electron precipitation events from 22:54:15 to 22:56:50 UT. The electron E > 45 keV trapping boundary is at 22:57:50 UT. ($Kp=2^-$.)

Figure 12 Frequency-time spectrograms showing two downgoing V-shaped VLF hiss events and an upgoing saucer emission associated with the inverted 'V' precipitation events shown in Figure 9.

Figure 13 Illustrative model showing the generation regions of VLF hiss and saucer emissions and their relationship to precipitating magnetosheath electrons and upgoing low energy ionospheric electrons.

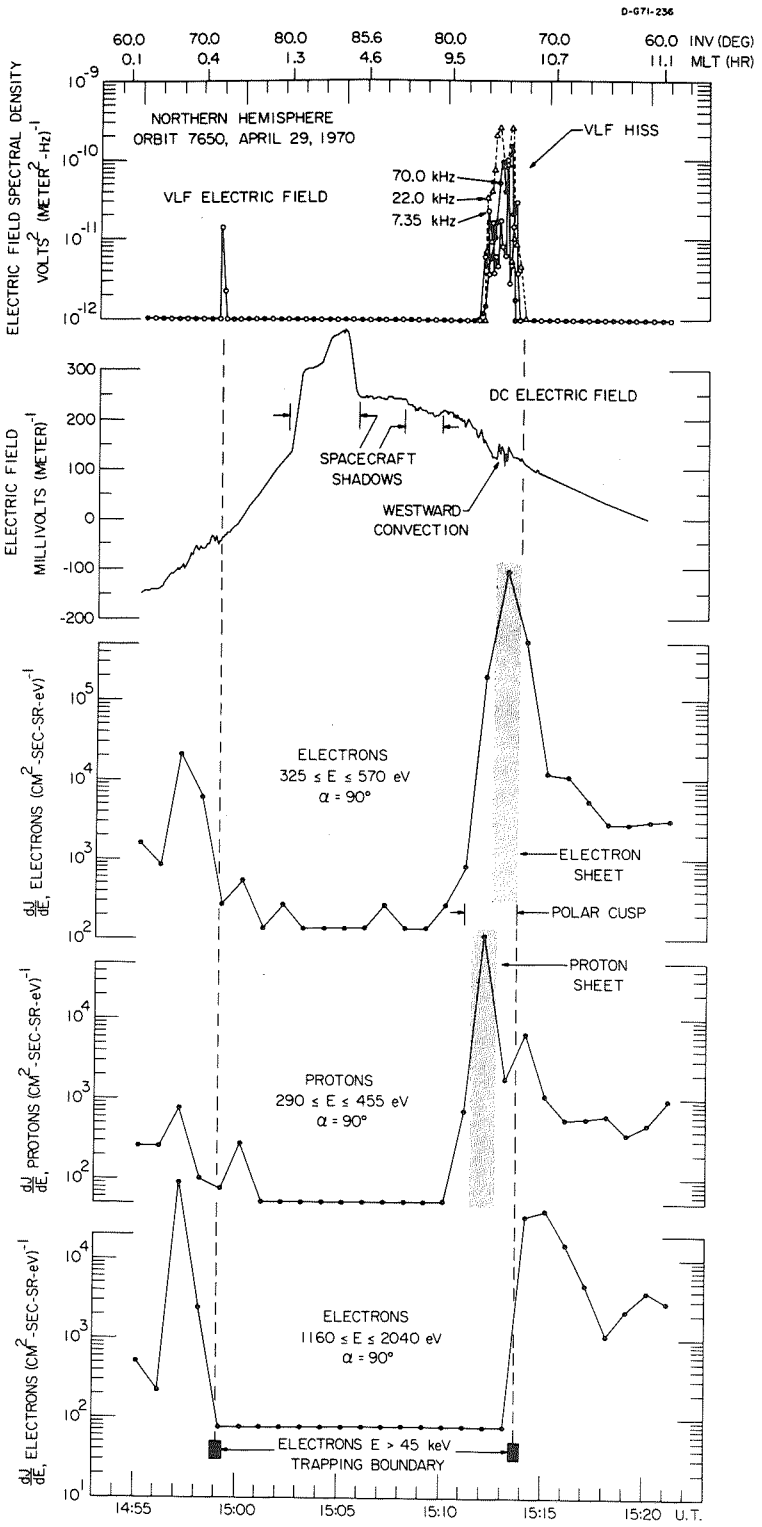
D-G71-236
60.0 0.1
70.0 0.4
80.0 1.3
85.6 4.6
80.0 9.5
70.0 10.7
60.0 11.1 INV (DEG) MLT (HR)
ELECTRIC FIELD SPECTRAL DENSITY VOLTS^2 (METER^2-Hz)$^{-1}$
NORTHERN HEMISPHERE
ORBIT 7650, APRIL 29, 1970
VLF HISS
VLF ELECTRIC FIELD
70.0 kHz
22.0 kHz
7.35 kHz
ELECTRIC FIELD MILLIVOLTS (METER)$^{-1}$
DC ELECTRIC FIELD
SPACECRAFT SHADOWS
WESTWARD CONVECTION
$\frac{dJ}{dE}$, ELECTRONS (CM^2-SEC-SR-eV)$^{-1}$
ELECTRONS
325 ≤ E ≤ 570 eV
α = 90°
ELECTRON SHEET
POLAR CUSP
PROTON SHEET
$\frac{dJ}{dE}$, PROTONS (CM^2-SEC-SR-eV)$^{-1}$
PROTONS
290 ≤ E ≤ 455 eV
α = 90°
$\frac{dJ}{dE}$, ELECTRONS (CM^2-SEC-SR-eV)$^{-1}$
ELECTRONS
1160 ≤ E ≤ 2040 eV
α = 90°
ELECTRONS E > 45 keV
TRAPPING BOUNDARY
14:55
15:00
15:05
15:10
15:15
15:20 U.T.

Figure 1

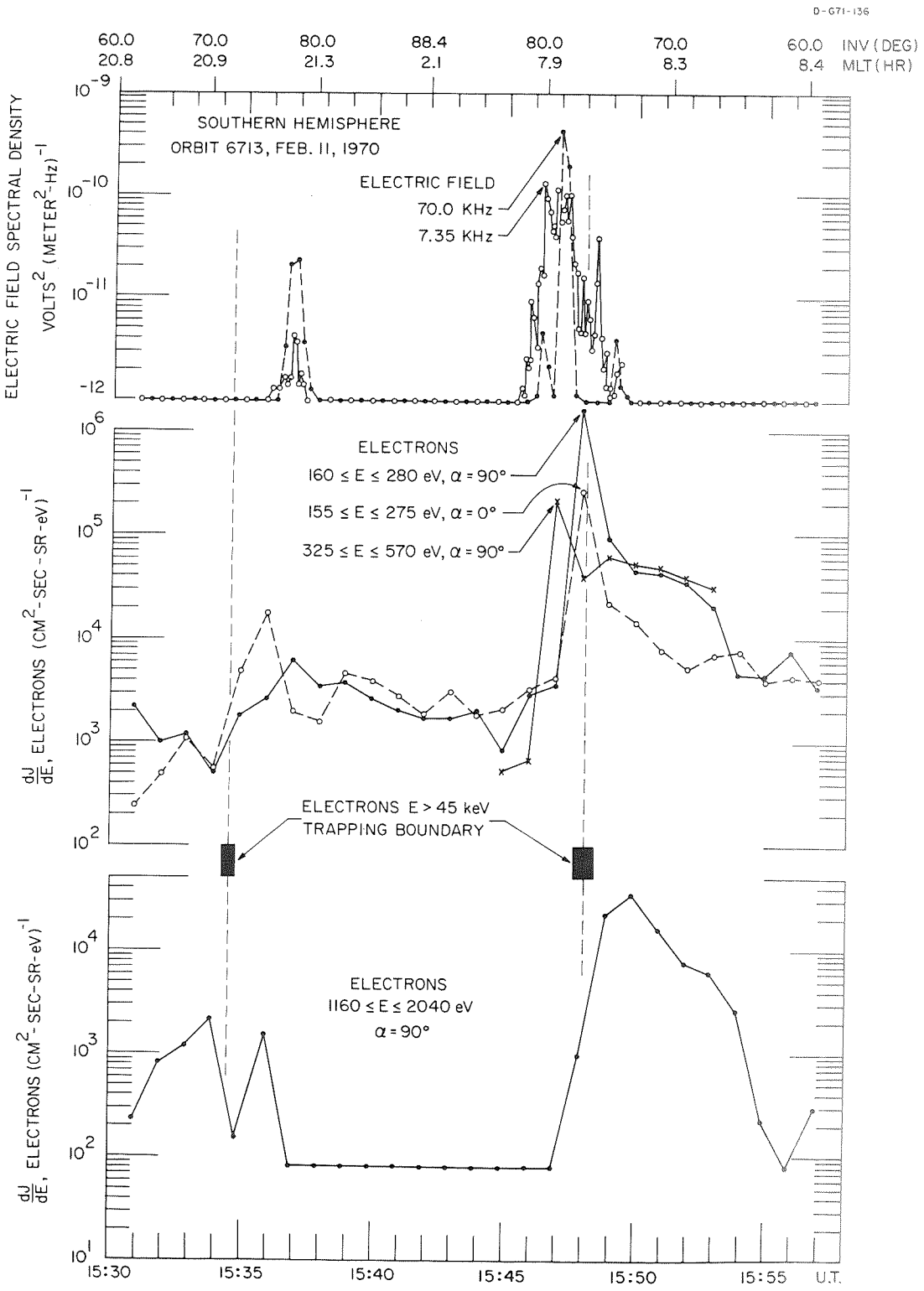
D-G71-136
60.0 20.8
70.0 20.9
80.0 21.3
88.4 2.1
80.0 7.9
70.0 8.3
60.0 8.4
INV (DEG)
MLT (HR)
SOUTHERN HEMISPHERE
ORBIT 6713, FEB. 11, 1970
ELECTRIC FIELD SPECTRAL DENSITY
VOLTS^2 (METER^2-Hz)$^{-1}$
ELECTRIC FIELD
70.0 KHz
7.35 KHz
ELECTRONS
160 ≤ E ≤ 280 eV, α = 90°
155 ≤ E ≤ 275 eV, α = 0°
325 ≤ E ≤ 570 eV, α = 90°
dJ/dE, ELECTRONS (CM^2-SEC-SR-eV)$^{-1}$
ELECTRONS E > 45 keV
TRAPPING BOUNDARY
ELECTRONS
1160 ≤ E ≤ 2040 eV
α = 90°
15:30
15:35
15:40
15:45
15:50
15:55
U.T.

Figure 2

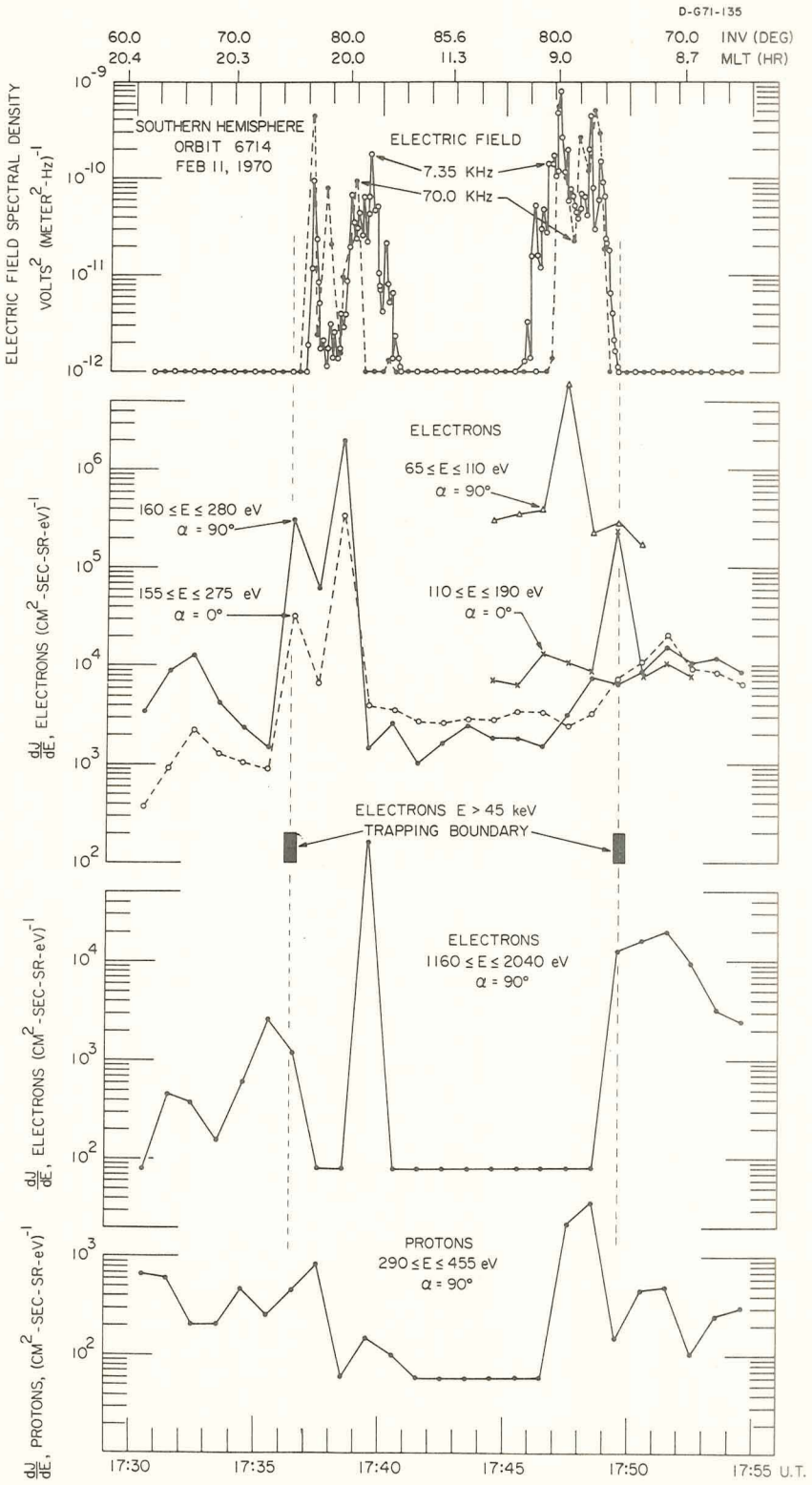
D-G71-135
60.0 70.0 80.0 85.6 80.0 70.0 INV (DEG)
20.4 20.3 20.0 11.3 9.0 8.7 MLT (HR)
ELECTRIC FIELD SPECTRAL DENSITY VOLTS^2 (METER^2-Hz)$^{-1}$
SOUTHERN HEMISPHERE
ORBIT 6714
FEB 11, 1970
ELECTRIC FIELD
7.35 KHz
70.0 KHz
ELECTRONS
65 ≤ E ≤ 110 eV
α = 90°
160 ≤ E ≤ 280 eV
α = 90°
110 ≤ E ≤ 190 eV
α = 0°
155 ≤ E ≤ 275 eV
α = 0°
dJ/dE, ELECTRONS (CM^2-SEC-SR-eV)$^{-1}$
ELECTRONS E > 45 keV
TRAPPING BOUNDARY
ELECTRONS
1160 ≤ E ≤ 2040 eV
α = 90°
dJ/dE, ELECTRONS (CM^2-SEC-SR-eV)$^{-1}$
PROTONS
290 ≤ E ≤ 455 eV
α = 90°
dJ/dE, PROTONS, (CM^2-SEC-SR-eV)$^{-1}$
17:30 17:35 17:40 17:45 17:50 17:55 U.T.

Figure 3

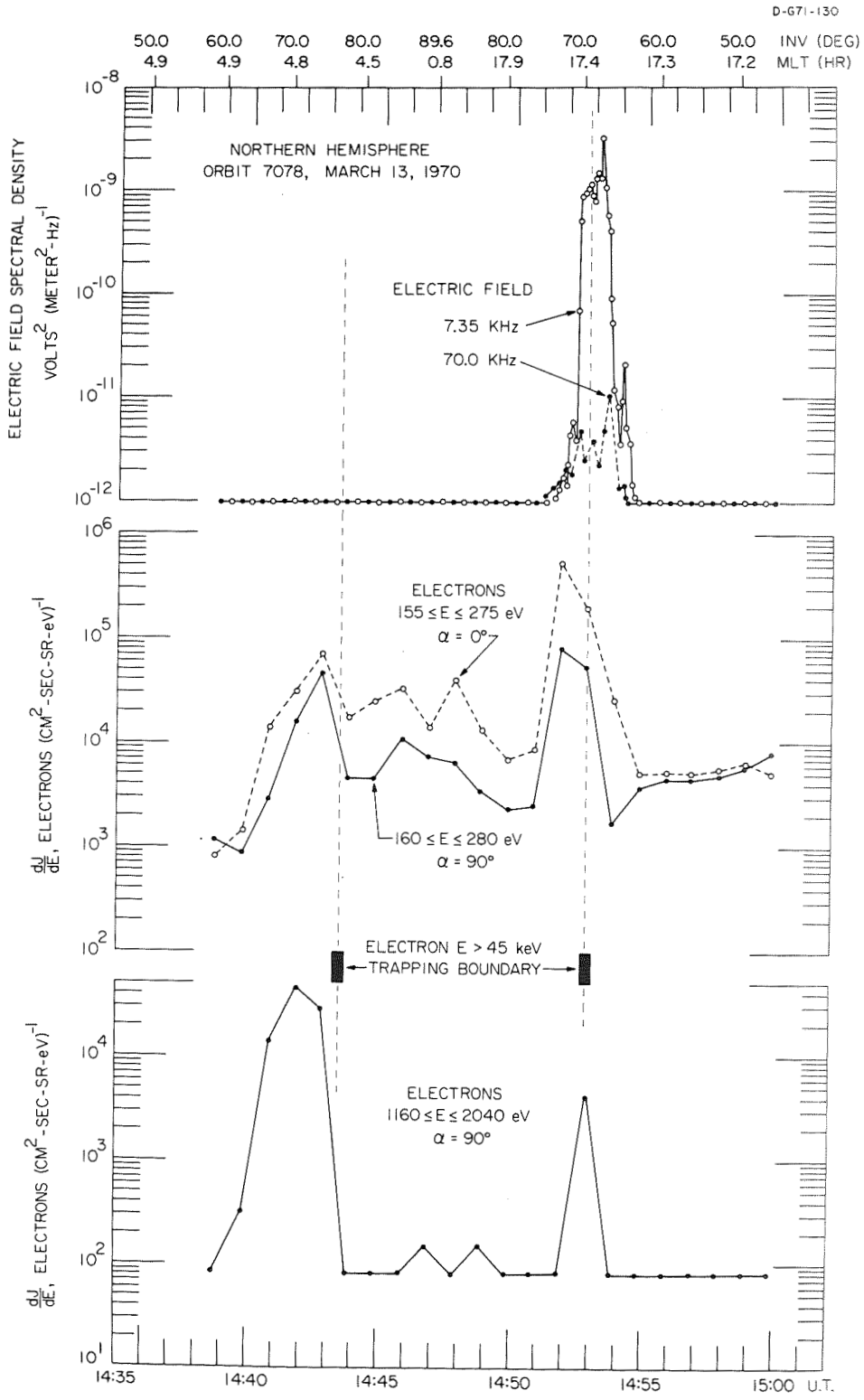
D-G71-130
50.0 4.9
60.0 4.9
70.0 4.8
80.0 4.5
89.6 0.8
80.0 17.9
70.0 17.4
60.0 17.3
50.0 17.2
INV (DEG)
MLT (HR)
NORTHERN HEMISPHERE
ORBIT 7078, MARCH 13, 1970
ELECTRIC FIELD SPECTRAL DENSITY
VOLTS^2 (METER^2-Hz)$^{-1}$
ELECTRIC FIELD
7.35 KHz
70.0 KHz
ELECTRONS
155 ≤ E ≤ 275 eV
α = 0°
160 ≤ E ≤ 280 eV
α = 90°
dJ/dE, ELECTRONS (CM^2-SEC-SR-eV)$^{-1}$
ELECTRON E > 45 keV
TRAPPING BOUNDARY
ELECTRONS
1160 ≤ E ≤ 2040 eV
α = 90°
14:35
14:40
14:45
14:50
14:55
15:00 U.T.

Figure 4

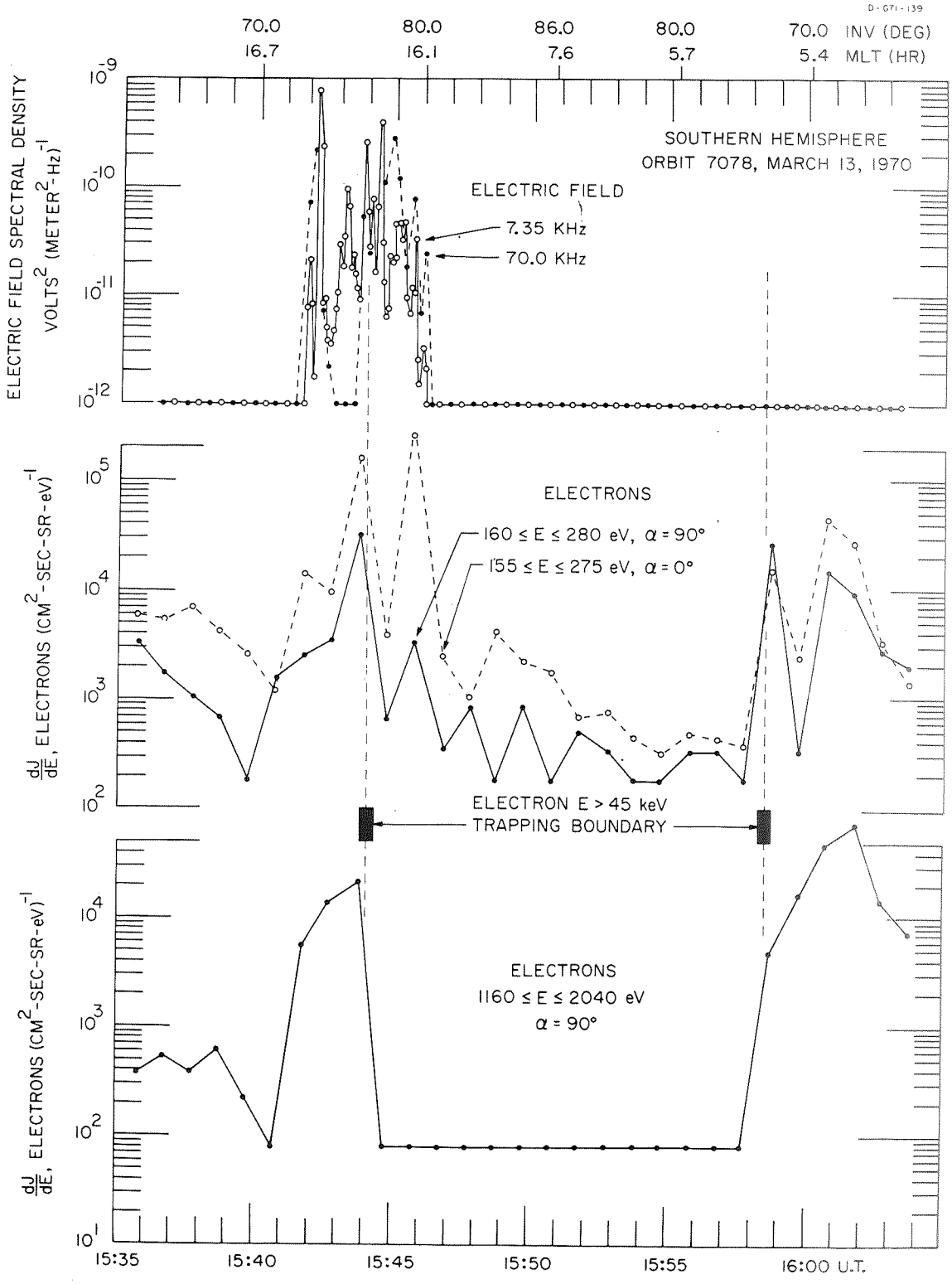
D-671-139
70.0 INV (DEG)
16.7
80.0
16.1
86.0
7.6
80.0
5.7
70.0
5.4 MLT (HR)
SOUTHERN HEMISPHERE
ORBIT 7078, MARCH 13, 1970
ELECTRIC FIELD SPECTRAL DENSITY
VOLTS^2 (METER^2-Hz)$^{-1}$
ELECTRIC FIELD
7.35 KHz
70.0 KHz
ELECTRONS
160 ≤ E ≤ 280 eV, α = 90°
155 ≤ E ≤ 275 eV, α = 0°
$\frac{dJ}{dE}$, ELECTRONS (CM^2-SEC-SR-eV)$^{-1}$
ELECTRON E > 45 keV
TRAPPING BOUNDARY
ELECTRONS
1160 ≤ E ≤ 2040 eV
α = 90°
15:35
15:40
15:45
15:50
15:55
16:00 U.T.

Figure 5

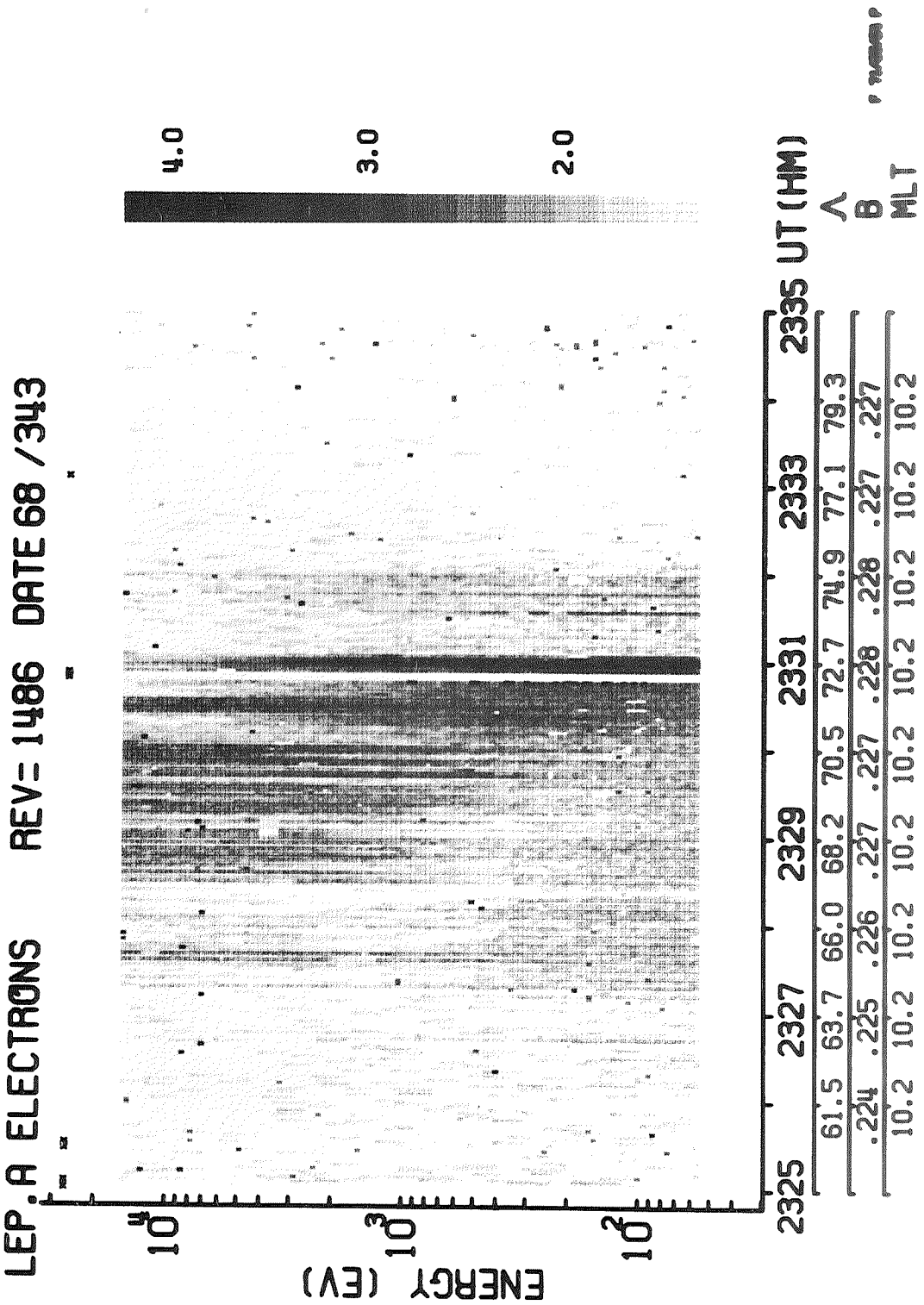
LEP.A ELECTRONS REV=1486 DATE 68/343
4.0
3.0
2.0
ENERGY (EV)
10^4
10^3
10^2
2325 2327 2329 2331 2333 2335 UT(HM)
Λ
B
MLT

Figure 6

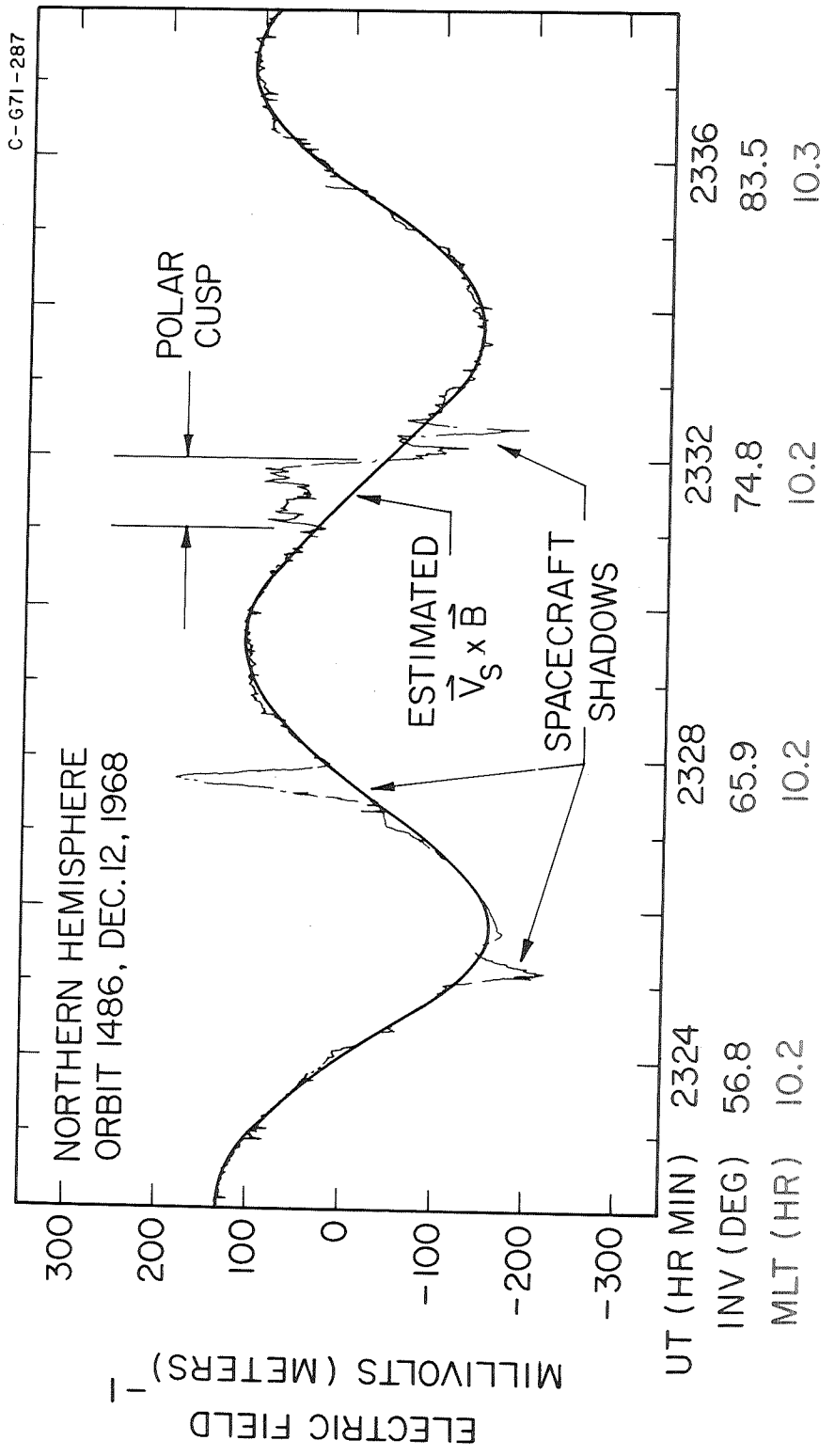
C-G71-287
NORTHERN HEMISPHERE
ORBIT 1486, DEC. 12, 1968
POLAR
CUSP
ESTIMATED
$\vec{V}_S \times \vec{B}$
SPACECRAFT
SHADOWS
ELECTRIC FIELD
MILLIVOLTS (METERS)$^{-1}$
300
200
100
0
-100
-200
-300
UT (HR MIN) 2324 2328 2332 2336
INV (DEG) 56.8 65.9 74.8 83.5
MLT (HR) 10.2 10.2 10.2 10.3

Figure 7

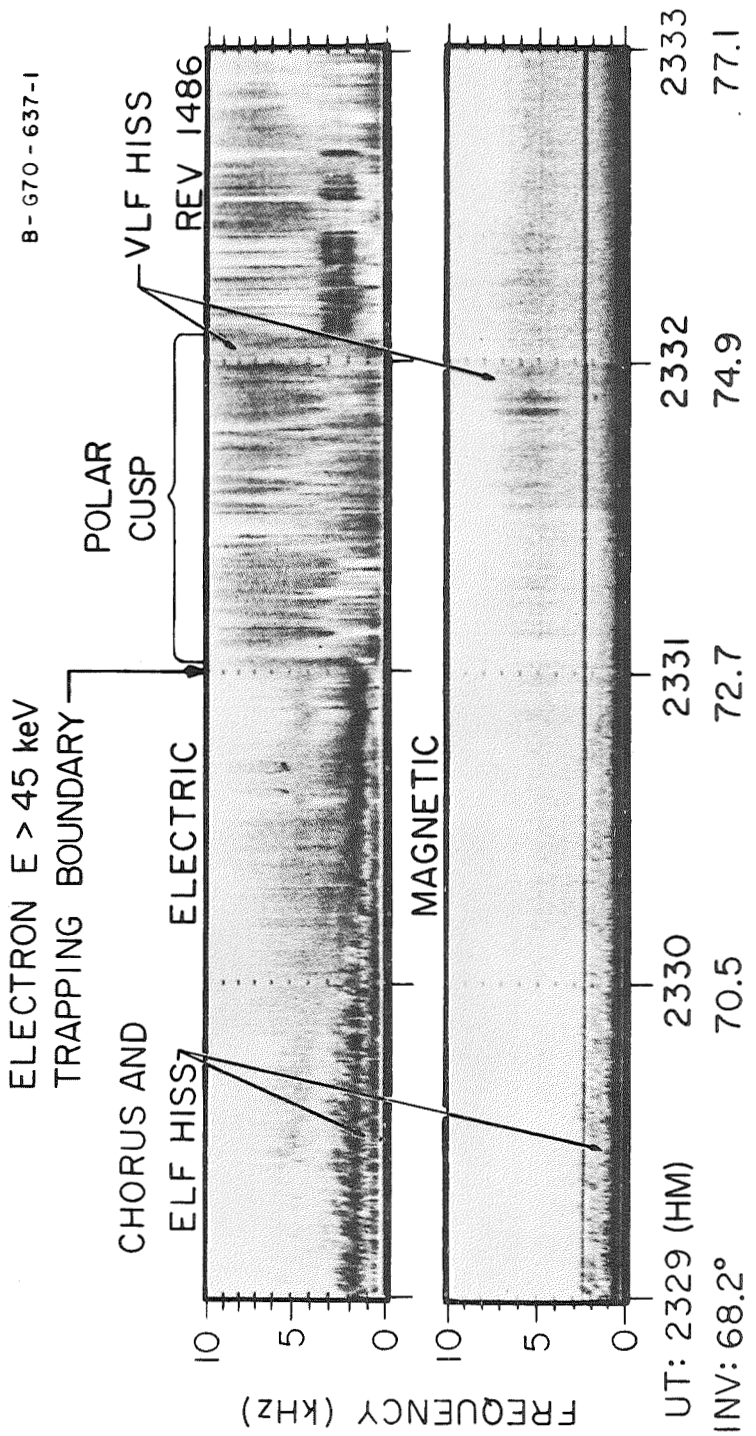
B-G70-637-1
ELECTRON E > 45 keV
TRAPPING BOUNDARY
POLAR
CUSP
VLF HISS
REV 1486
CHORUS AND
ELF HISS
ELECTRIC
MAGNETIC
FREQUENCY (kHz)
10
5
0
UT: 2329 (HM)
2330
2331
2332
2333
INV: 68.2°
70.5
72.7
74.9
77.1

Figure 8

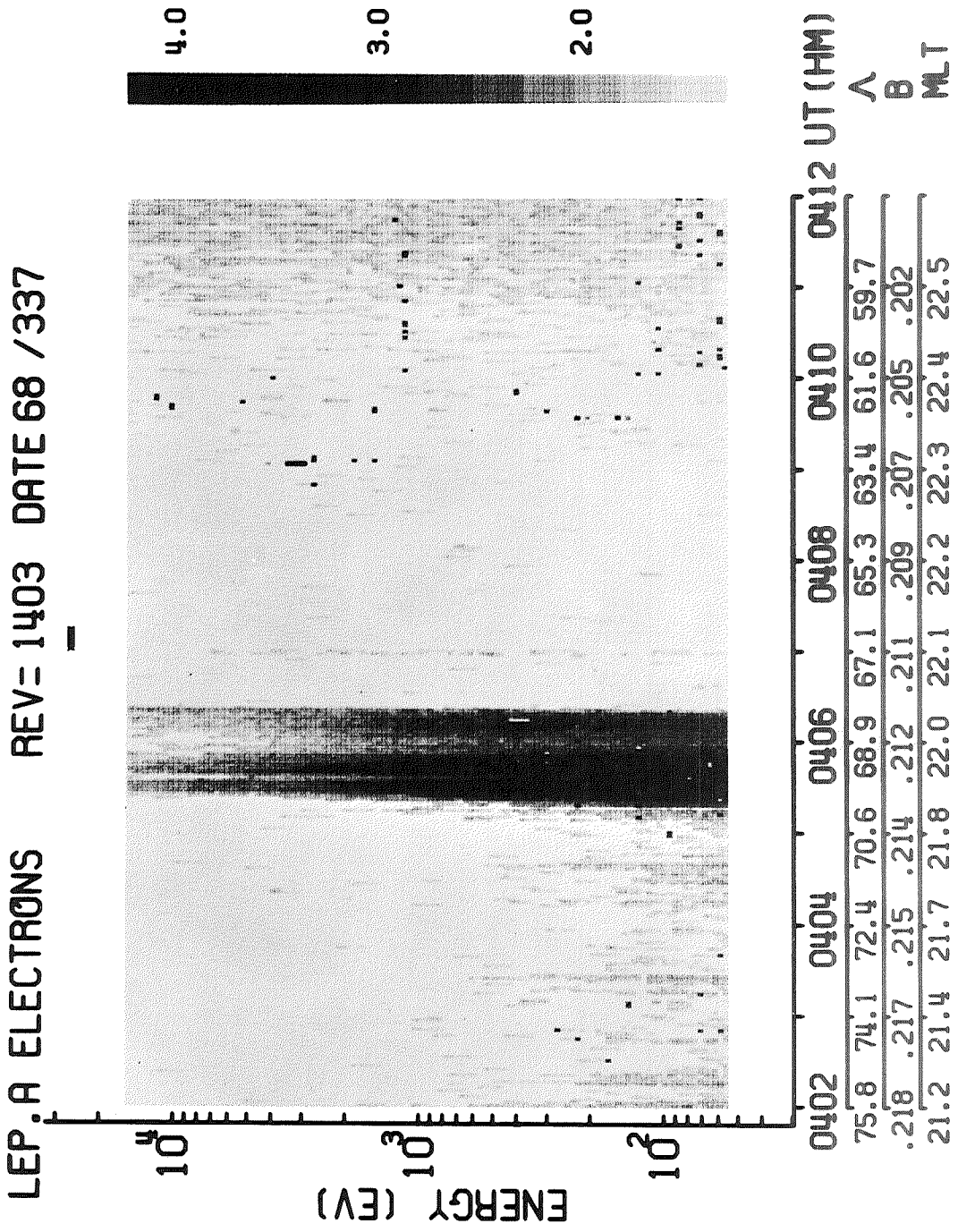
LEP.A ELECTRONS REV= 1403 DATE 68 /337
ENERGY (EV)
10^4
10^3
10^2
4.0
3.0
2.0
0402 0404 0406 0408 0410 0412 UT(HM)
A
B
MLT
75.8 74.1 72.4 70.6 68.9 67.1 65.3 63.4 61.6 59.7
.218 .217 .215 .214 .212 .211 .209 .207 .205 .202
21.2 21.4 21.7 21.8 22.0 22.1 22.2 22.3 22.4 22.5

Figure 9

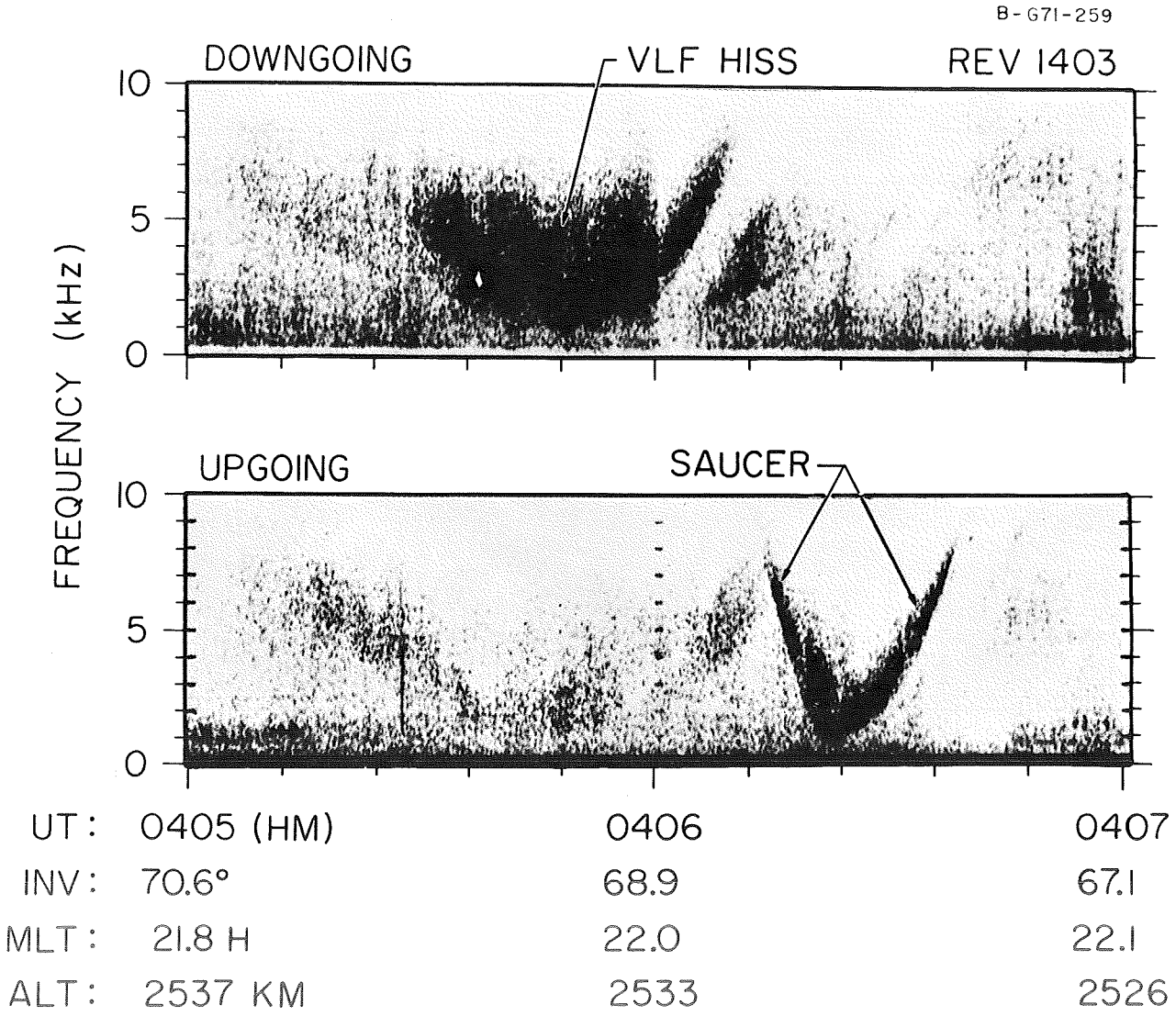
B-G71-259
DOWNGOING
VLF HISS
REV 1403
10
5
0
FREQUENCY (kHz)
UPGOING
SAUCER
10
5
0
UT: 0405 (HM) 0406 0407
INV: 70.6° 68.9 67.1
MLT: 21.8 H 22.0 22.1
ALT: 2537 KM 2533 2526

Figure 10

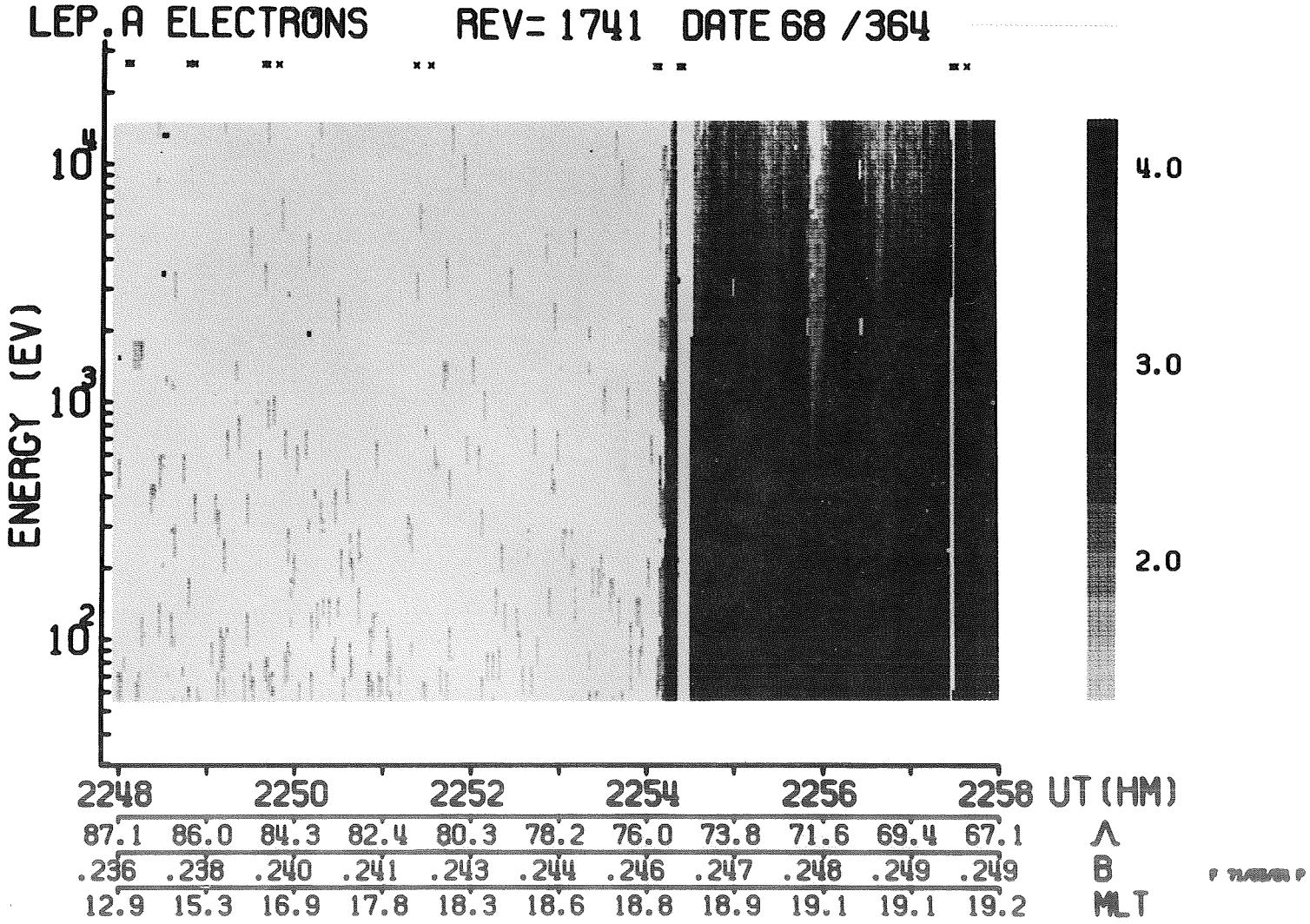
LEP.A ELECTRONS REV= 1741 DATE 68 /364
ENERGY (EV)
10⁴
10³
10²
4.0
3.0
2.0
2248
2250
2252
2254
2256
2258 UT (HM)
87.1 86.0 84.3 82.4 80.3 78.2 76.0 73.8 71.6 69.4 67.1 Λ
.236 .238 .240 .241 .243 .244 .246 .247 .248 .249 .249 B
12.9 15.3 16.9 17.8 18.3 18.6 18.8 18.9 19.1 19.1 19.2 MLT

Figure 11

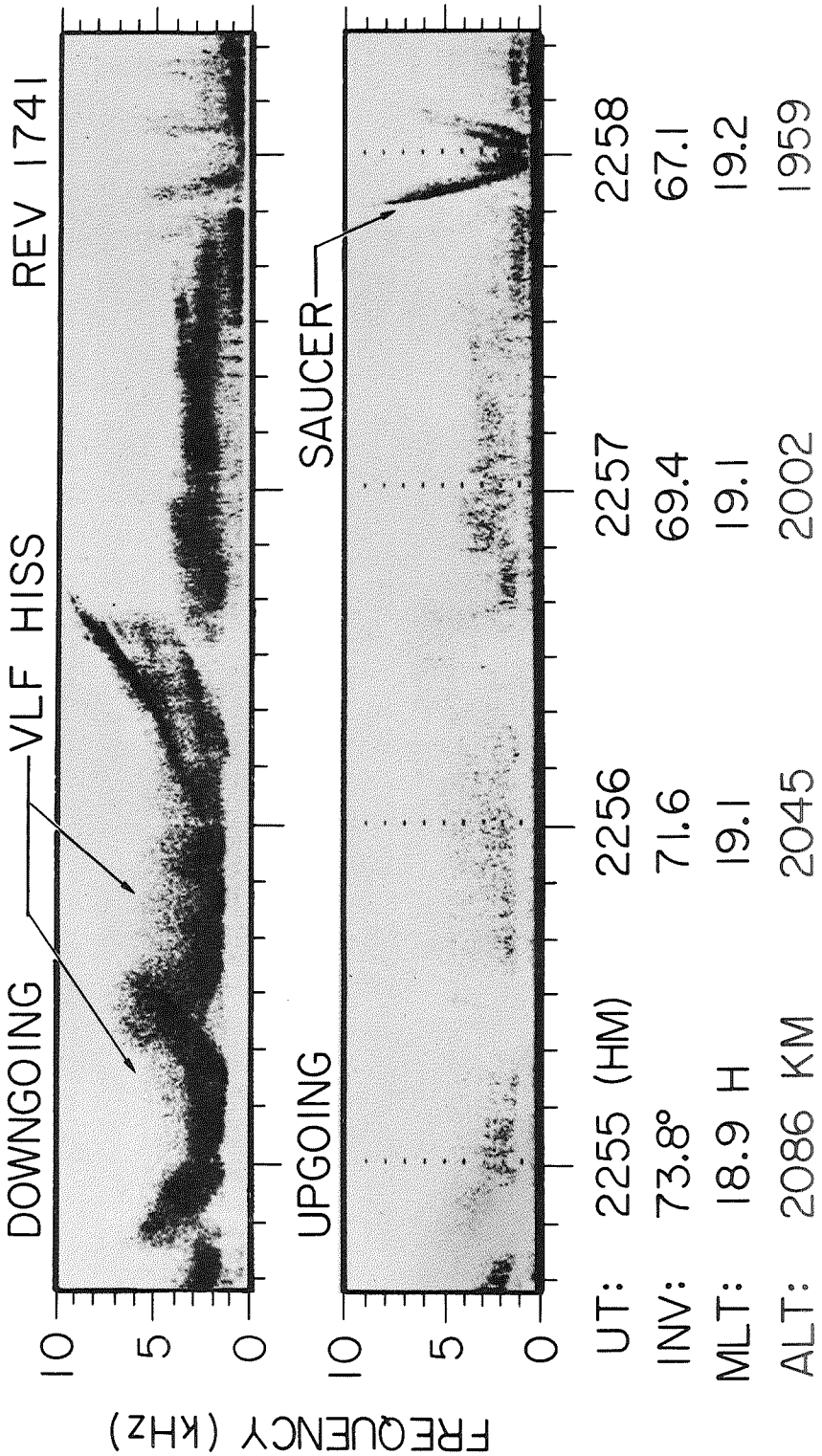
B-G71-260
REV 1741
VLF HISS
DOWNGOING
SAUCER
UPGOING
FREQUENCY (kHz)
10
5
0
UT: 2255 (HM) 2256 2257 2258
INV: 73.8° 71.6 69.4 67.1
MLT: 18.9 H 19.1 19.1 19.2
ALT: 2086 KM 2045 2002 1959

Figure 12

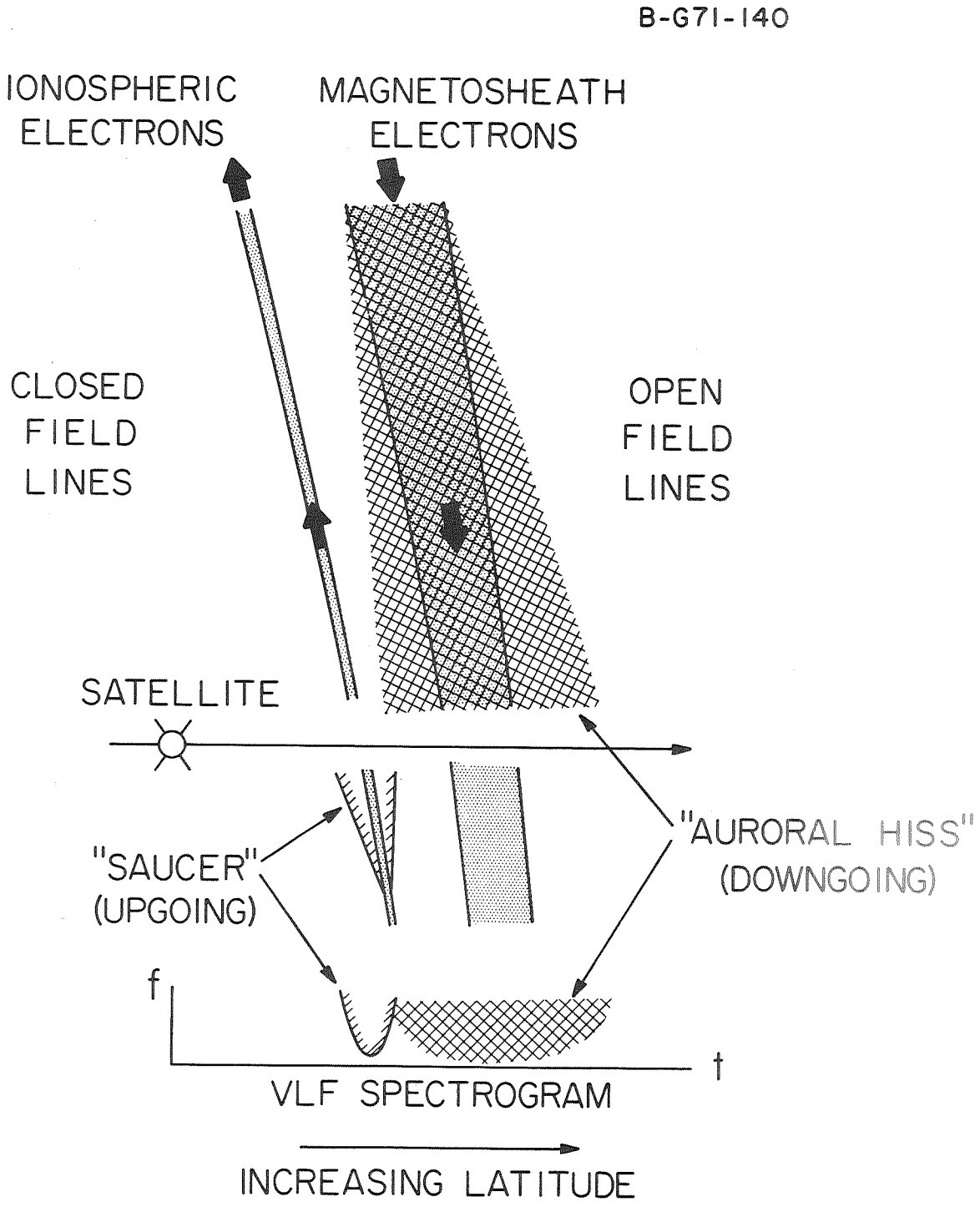
B-G71-140
IONOSPHERIC ELECTRONS
MAGNETOSHEATH ELECTRONS
CLOSED FIELD LINES
OPEN FIELD LINES
SATELLITE
"AURORAL HISS" (DOWNGOING)
"SAUCER" (UPGOING)
f
t
VLF SPECTROGRAM
INCREASING LATITUDE

Figure 13